Wave motions due to a point source pulsating and advancing at forward speed parallel to a semi-infinite ice sheet

Z. F. Li,[1] G. X. Wu,[2,*] and Y. Y. Shi[1]

[1]*School of Naval Architecture and Ocean Engineering, Jiangsu University of Science and Technology, Zhenjiang 212003, China*

[2]*Department of Mechanical Engineering, University College London, Torrington Place, London WC1E 7JE, United Kingdom*

(Received 15 May 2023; accepted 31 October 2023; published 5 January 2024)

The Green function, or the wave motion due to a point source pulsating and advancing at constant forward speed along a semi-infinite ice sheet in finite water depth is investigated, based on the linear velocity potential theory for fluid flow and thin elastic plate model for the ice sheet. The result is highly relevant to the ship motions near marginal seas. The ice edge is assumed to be free, or zero bending moment and shear-force conditions are used, while other edge conditions can be similarly considered. The Green function G is derived first through the Fourier transform along the direction of forward speed and then by the Wiener-Hopf technique along the transverse direction across both the free surface and ice sheet. The result shows that in the ice-covered domain, G can be decomposed into three parts. The first one is that upper ocean surface is fully covered by an ice sheet, and the second and third ones are due to the free surface and ice edge. Similarly, in the free-surface domain, G contains the component corresponding to that the upper water surface is fully free, while the second and third ones are due to the ice sheet and ice edge. In both domains, the latter two are due to the interactions of the free-surface wave and ice sheet deflection, which leads to the major complication. In-depth investigations are made for each part of G, and aim to shed some light on the nature of the wave motions induced by a ship advancing along a semi-infinite ice sheet at constant forward speed.

DOI: 10.1103/PhysRevFluids.9.014801

I. INTRODUCTION

Icy water regions have become a focal point for environmental protection and future developments due to the climate change. In the Arctic region especially, with the reduction of the ice extent and thickness, an overall uptrend of the wave height has been observed [1], and potentially a shipping route may become possible [2]. When a ship is advancing in marginal sea, it may navigate in open water along the edge of a large ice sheet to avoid the additional ice loads. Highly complex behavior of the ship motion can be expected, because of wave reflection and transmission at the edge of the ice sheet. To understand the nature of interactions between the ship and external environment is of important practical relevance. This work aims to shed some light on the behavior of wave motions due to a ship advancing along the edge of an ice sheet.

*Corresponding author: g.wu@ucl.ac.uk

Published by the American Physical Society under the terms of the Creative Commons Attribution 4.0 International license. Further distribution of this work must maintain attribution to the author(s) and the published article's title, journal citation, and DOI.

There has been extensive research on the wave interactions with a large ice sheet in the context of geophysics. Field experiment by Robin [3] suggested that a large ice sheet could bend to let the energy pass through. In many cases, the large ice sheet can be treated as an elastic plate, and the linear velocity potential theory can be used to describe the fluid flow [4]. When there is no ice sheet, the pressure on the water surface is assumed to be atmospheric and the wave is commonly called the free-surface wave [5]. For the water surface covered by an ice sheet, in addition to gravity, there is also force due to the flexural elasticity of the ice sheet, and the wave is commonly named the flexural-gravity wave [6]. As a free-surface wave in open water propagates to the ice-covered region in the form of a flexural-gravity wave, the energy will be partially reflected back due to the change of physical properties on the water surface. Based on the matched eigenfunction expansion (MEE) for finite water depth, Fox and Squire [7] solved the two-dimensional (2D) problem of wave interaction with a semi-infinite ice sheet, in which the unknowns were computed through the conjugate gradient method to minimize the error function. During the wave–ice interactions, Fox and Squire [8] showed numerically that the strain magnitudes for reasonable wave heights were sufficient to break up the ice sheet. The case was later extended by Fox and Squire [9] to the oblique incident wave, and they confirmed that a critical angle existed if the wave number for free surface was larger than that for a flexural-gravity wave, similar to the Snell law. Sahoo *et al.* [10] introduced an orthogonal inner product to solve the unknowns of the eigenfunction expansions, and considered the effect of various ice-edge conditions, i.e., free edge, simply supported edge, and built-in edge. Chakrabarti [11] studied wave interactions with a semi-infinite ice sheet of infinite water depth by reducing the problem to that of a singular integral equation of the Carleman type over a semi-infinite range. For the problem of a semi-infinite free surface and a semi-infinite ice cover, the Wiener-Hopf technique (WHT) is an effective approach, as used by, e.g., Balmforth and Craster [12] and Tkacheva [13]. In Balmforth and Craster [12], it was shown that the Kirchhoff-Love model for a thin elastic plate would gave similar results to those by the Timoshenko-Mindlin model, within a typical range of ice properties and wave parameters. The scattering problem of water waves by a semi-infinite ice sheet was also solved by Linton and Chung [14] through the residue calculus technique.

The work on wave–ice–body interaction problem started only more recently, as new shipping routes and resource extractions in the Arctic would become more feasible in the coming decades [15]. For 2D wave interactions with a body in an ice polynya, Sturova [16] derived the corresponding Green function through MEE, and the radiation problem of a submerged cylinder was studied. The unknown coefficients in the eigenfunction expansions were recomputed for each source position. To improve the computation efficiency, the Green function was obtained by Sturova and Tkacheva [17] through WHT. For a rectangular barge floating on the polynya, Ren *et al.* [18] derived a semianalytical solution through MEE. By using the eigenfunction expansions in the two ice-covered regions and boundary integral equation in the polynya, Li *et al.* [19] developed a hybrid method for a 2D floating body of arbitrary shape. For a wide polynya, during the ice–body interactions, the evanescent wave mode from one body can be ignored near another body. Based on this assumption, Li *et al.* [20] further developed an approximate solution procedure, through which the nature of the oscillatory behavior of the hydrodynamic force was uncovered. For 3D wave–ice–body interaction problems, Ren *et al.* [21] derived a semianalytical solution for a bottom-mounted vertical circular cylinder in a circular polynya, and similar oscillatory behaviors of the hydrodynamic force to the 2D problem were found. For practical engineering problems, both the shapes of structure and polynya may be arbitrary. Li *et al.* [22] developed a 3D hybrid method in which a series of 2D integral equations in horizontal plane under the ice and a 3D integral equation in the polynya were constructed, and the matching solution was obtained through an orthogonal inner product. By using the Fourier transform along the straight ice edge of infinite length and MEE in the transverse plane, Li *et al.* [23] obtained the Green functions for an oscillating source in an ice channel and that near a semi-infinite ice sheet [24]. Because the Green function satisfies all the

boundary conditions except that on the body surface, when the governing differential equation is converted into an integral equation over the boundary, only the integral over the body surface needs to be kept, which means that only the body surface needs to be discretized in numerical calculation.

The above work is mainly about the interactions between ocean waves and a body with zero forward speed. For a ship advancing at constant speed along a straight line in open water, the Kelvin wave in V shape can be observed behind the ship. The wave consists of transverse and divergent components, confined within an angle of $\arcsin(1/3)$ in deep water [5]. If the surface-tension effect is considered, Liang and Chen [25] found that the divergent capillary-gravity waves would disappear for some particular surface tension coefficients and speed of the disturbance. In addition to the Kelvin angle, Rabaud and Moisy [26] observed the angle corresponding to the maximum of the amplitude of the waves for real ships, which decreases as the reciprocal of the speed at large velocities. This was then studied theoretically in Ref. [27] through an axisymmetric moving pressure. When there is an ice sheet on the water surface, the wave system will be very much different. By using the asymptotic Fourier analysis, Davys *et al.* [28] studied the steady wave patterns generated by a steadily moving source on the ice sheet, and found that the waves with larger group velocity dominated by elasticity propagate ahead, and the waves with smaller group velocity follow behind. From the field experiment, Takizawa [29] also observed the two wave systems, respectively, ahead and behind the moving load, when the speed is larger than the critical one. Milinazzo *et al.* [30] derived an analytical solution to the steady flexural-gravity wave induced by the uniform motion of a rectangular load, which was expressed in the form of a Fourier integral. It was suggested that the solution might be unbounded at the critical speed. For an ice sheet confined within boundaries, Shishmarev *et al.* [31] studied the deflection of an ice sheet in a water channel bounded by two parallel vertical walls with clamped edge condition. Fourier transform was used along the channel and eigenmode expansion was adopted across the channel. Based on WHT, Tkacheva [32] derived an analytical solution for a uniformly moving load on a semi-infinite ice sheet, and the deflection of the ice sheet as well as the elevation of the free-surface wave were investigated. The solution procedure was then extended to a moving pressure on an infinitely extended ice sheet with a crack [33], and in a channel confined by two semi-infinite ice sheet [34].

In this work, we consider the Green function or the velocity potential induced by a pulsating source advancing at a uniform forward speed along a semi-infinite ice sheet. Through the solution of the Green function itself, we can acquire some in-depth understanding of wave interactions with a body moving in the marginal ice zone. In a much wider context, with the help of the Green function, the boundary integral equation can be derived for a practical ship, and the hydrodynamic problem can be solved numerically through the boundary element method, as in the fully free-surface problem. To solve the problem, we first perform the Fourier transform in the forward speed direction. WHT is then used in the transverse direction. When the field point is in the ice-covered (free-surface) part, the Green function can be written as a combination of the Green function for infinite ice sheet (free surface) and two parts arising from the ice edge and the semi-infinite free surface (ice sheet). In each of these cases, details of the wave pattern can then be analyzed and the natures of the wave can be understood.

In the following sections, the mathematical model is formulated in Sec. II, and the governing equation for the Green function together with the boundary conditions are described. In Sec. III, the detailed procedure of WHT for this problem is given, and the solution of the Green function is provided. Then, the formulations for ice-sheet deflection and free-surface wave elevation are given in Sec. IV. Results are provided and discussed in Sec. V, followed by the conclusions in Sec. VI. In Appendix A, the roots of the dispersion equation are given, while Appendix B gives the factorization of the dispersion equation. Appendix C provides the computation of matrix equation from the WHT. Special case for an infinite ice sheet and an infinite free surface is given in Appendix D. Finally, wave feature at the far field is derived in Appendix E.

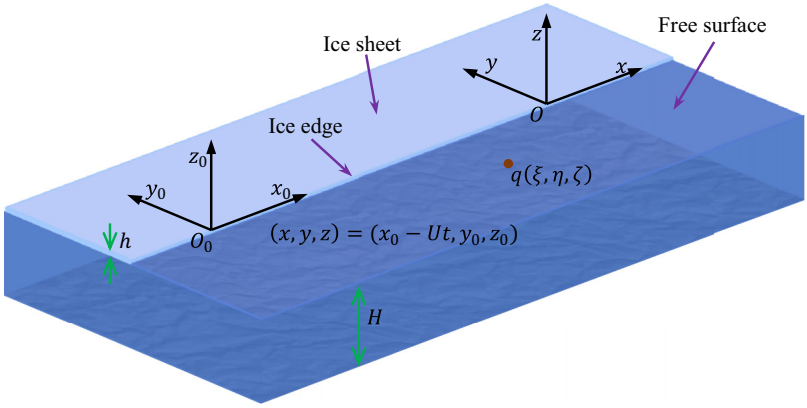

FIG. 1. Coordinate system and sketch of the problem.

II. MATHEMATICAL MODEL

As sketched in Fig. 1, we consider the wave motions due to a point source pulsating with encounter radian frequency ω, and advancing at a constant forward speed U, parallel to the rectilinear edge of a semi-infinite ice sheet. This is related to the engineering problem of a ship advancing in waves in marginal sea. To describe the problem, two Cartesian coordinate systems are defined. One is the earth fixed coordinate system $O_0 - x_0y_0z_0$, with the x_0 axis along the straight edge of the semi-infinite ice sheet, z_0 axis pointing vertically upwards from the undisturbed water surface, and y_0 axis pointing into the ice sheet. The other is the coordinate system $O{-}xyz$, which moves with the same forward speed as that of the source. The two coordinate systems are related through the following equations:

$$(x, y, z) = (x_0 - Ut, y_0, z_0), \tag{2.1}$$

where t denotes the time.

The fluid is assumed to be inviscid, incompressible, and homogeneous, and its motion to be irrotational. Thus, the velocity potential ϕ can be introduced to describe the fluid flow. Based on the assumption that the amplitude of wave motion is small compared to its length, the linearized velocity potential theory can be further applied. For an oscillating source at a point $q(\xi, \eta, \zeta)$, the velocity potential ϕ at a field point $p(x, y, z)$ can be written as

$$\phi = \mathrm{Re}[G(p, q)e^{i\omega t}], \tag{2.2}$$

where G is commonly known as the Green function [5]. G should satisfy the following governing equation:

$$\nabla^2 G + \frac{\partial^2 G}{\partial z^2} = -4\pi\delta(x-\xi)\delta(y-\eta)\delta(z-\zeta), \tag{2.3}$$

throughout the fluid domain, where $\delta(x)$ is the Dirac delta function, and ∇^2 is the two-dimensional Laplacian operator with respect to x and y. The ice sheet is modeled as a thin elastic plate with uniform properties, with its draft effect being ignored [12]. Then, the equation of motion for the vertical deflection w of the ice sheet can be written as [35]

$$\left(L\nabla_0^4 + m\frac{\partial^2}{\partial t^2}\right)w = p \quad (y_0 \geqslant 0^+ \text{ and } z_0 = 0), \tag{2.4}$$

where $\nabla_0^4 = \nabla_0^2(\nabla_0^2)$, and ∇_0^2 is the two-dimensional Laplacian with respect to x_0 and y_0; $L = Eh^3/[12(1-\nu^2)]$ is the effective flexural rigidity of the ice sheet with E and ν, respectively, as

its Young's modulus and Poisson's ratio; $m = \rho_i h$ is the mass per unit area of the ice sheet with ρ_i as its density; and p is the difference of water pressure and atmosphere pressure on the ice sheet. During the ice-sheet deflection, it is assumed that there is no gap between the ice sheet and water upper surface. Through the linearized Bernoulli equation, the pressure p in Eq. (2.4) can be obtained by

$$p = -\rho_w\left(\frac{\partial\phi}{\partial t} + gw\right), \tag{2.5}$$

where ρ_w is the density of water and g is the acceleration due to gravity. The kinematic condition on their interface requires that the fluid-particle velocity in the normal direction of the ice sheet should be equal to that of ice-sheet deflection, i.e.,

$$\frac{\partial\phi}{\partial z_0} - \frac{\partial w}{\partial t} = 0 \quad (z_0 = 0). \tag{2.6}$$

Substituting Eq. (2.5) into (2.4), and using Eq. (2.6), we have

$$\left(L\nabla_0^4 + m\frac{\partial^2}{\partial t^2} + \rho_w g\right)\frac{\partial\phi}{\partial z_0} + \rho_w\frac{\partial^2\phi}{\partial t^2} = 0 \quad (y_0 \geqslant 0^+ \text{ and } z_0 = 0). \tag{2.7}$$

For $y_0 \leqslant 0^-$ and $z_0 = 0$, w represents the elevation of the free surface on which $p = 0$. We have

$$g\frac{\partial\phi}{\partial z_0} + \frac{\partial^2\phi}{\partial t^2} = 0 \quad (y_0 \leqslant 0^- \text{ and } z_0 = 0). \tag{2.8}$$

Using Eq. (2.1) and noticing

$$\left.\frac{\partial}{\partial t}\right|_{(x_0,y_0,z_0)} = \left.\frac{\partial}{\partial t}\right|_{(x,y,z)} - U\frac{\partial}{\partial x}, \tag{2.9}$$

Equations (2.7) and (2.8) can be also written as

$$\left[L\nabla^4 + m\left(\frac{\partial}{\partial t} - U\frac{\partial}{\partial x}\right)^2 + \rho_w g\right]\frac{\partial\phi}{\partial z} + \rho_w\left(\frac{\partial}{\partial t} - U\frac{\partial}{\partial x}\right)^2\phi = 0 \quad (y \geqslant 0^+ \text{ and } z = 0), \tag{2.10}$$

and

$$g\frac{\partial\phi}{\partial z} + \left(\frac{\partial}{\partial t} - U\frac{\partial}{\partial x}\right)^2\phi = 0 \quad (y \leqslant 0^- \text{ and } z = 0). \tag{2.11}$$

Here, the removal of the subscript 0 indicates that the partial derivatives with respect to (x_0, y_0, z_0) have been replaced by those to (x, y, z). At the edge of the semi-infinite ice sheet, zero bending moment and shear-force edge conditions are assumed, while other edge conditions can be considered in a similar way. This, together with Eqs. (2.6) and (2.9), provides

$$\mathcal{B}\left(\frac{\partial\phi}{\partial z}\right) = 0 \quad \text{and } \mathcal{S}\left(\frac{\partial\phi}{\partial z}\right) = 0 \quad (y = 0^+ \text{ and } z = 0), \tag{2.12}$$

where the operators $\mathcal{B}$ and $\mathcal{S}$ are defined as

$$\mathcal{B} = \frac{\partial^2}{\partial y^2} + \nu\frac{\partial^2}{\partial x^2} \quad \text{and } \mathcal{S} = \frac{\partial}{\partial y}\left[\frac{\partial^2}{\partial y^2} + (2-\nu)\frac{\partial^2}{\partial x^2}\right]. \tag{2.13}$$

It may be noticed that $y = 0^+$ and $y = 0^-$ with $z = 0$ indicate that the line is approached from the ice-sheet side and free-surface side, respectively. The fluid is assumed to have uniform depth H, and the impermeable boundary condition requires that

$$\frac{\partial\phi}{\partial z} = 0\,(z = -H). \tag{2.14}$$

In the far field or $x^2 + y^2 \to +\infty$, the radiation condition should be also imposed, stating that the radiated waves are outgoing.

III. SOLUTION PROCEDURE FOR THE GREEN FUNCTION

To derive the Green function G, we first introduce a negative imaginary part or $-i\epsilon$ to the radian frequency ω. The role of ϵ with $\epsilon \to 0^+$ is to ensure that the radiation condition is satisfied at the far field in a manner described by Lighthill [36]. We introduce the dimensionless variables based on the three basic parameters, i.e., density of water ρ_w, acceleration due to gravity g, and a characteristic length l. Thus,

$$D = \frac{L}{\rho_w g l^4}, \quad M = \frac{m}{\rho_w l}, \quad \varepsilon = \frac{\epsilon}{\sqrt{g/l}}, \quad f = \frac{\omega}{\sqrt{g/l}}, \quad F = \frac{U}{\sqrt{gl}}, \tag{3.1}$$

together with $(\hat{x}, \hat{y}, \hat{z}) = (x, y, z)/l$, $(\hat{\xi}, \hat{\eta}, \hat{\zeta}) = (\xi, \eta, \zeta)/l$, and $\hat{H} = H/l$. In the following text, the over-hat in the spatial coordinates will be omitted. Substituting Eq. (2.2) into Eqs. (2.10), (2.11), (2.12), and (2.14), we have

$$\left[D\nabla^4 - M\left(f - i\varepsilon + iF\frac{\partial}{\partial x}\right)^2 + 1\right]\frac{\partial G}{\partial z} - \left(f - i\varepsilon + iF\frac{\partial}{\partial x}\right)^2 G = 0 \quad (y \geqslant 0^+ \text{ and } z = 0), \tag{3.2}$$

$$\frac{\partial G}{\partial z} - \left(f - i\varepsilon + iF\frac{\partial}{\partial x}\right)^2 G = 0 \quad (y \leqslant 0^- \text{and } z = 0), \tag{3.3}$$

$$\mathcal{B}\left(\frac{\partial G}{\partial z}\right) = 0 \quad \text{and } \mathcal{S}\left(\frac{\partial G}{\partial z}\right) = 0 \quad (y = 0^+ \text{ and } z = 0), \tag{3.4}$$

$$\frac{\partial G}{\partial z} = 0 \quad (z = -H). \tag{3.5}$$

In order to derive G, we use the following double Fourier transform:

$$\widehat{G}(\alpha, y, z) = \frac{1}{\sqrt{2\pi}}\int_{-\infty}^{+\infty} G(x, y, z)e^{i\alpha x}dx, \tag{3.6}$$

$$\tilde{G}(\alpha, \beta, z) = \frac{1}{\sqrt{2\pi}}\int_{-\infty}^{+\infty} \widehat{G}(\alpha, y, z)e^{i\beta y}dy, \tag{3.7}$$

in the horizontal O-xy plane. Equations (2.3) and (3.5) become

$$-k^2\tilde{G} + \frac{\partial^2\tilde{G}}{\partial z^2} = -2e^{i\alpha\xi}e^{i\beta\eta}\delta(z - \zeta), \tag{3.8}$$

$$\frac{\partial\tilde{G}}{\partial z} = 0 \quad (z = -H), \tag{3.9}$$

where

$$(\alpha, \beta) = k(\cos\ \theta, \sin\ \theta). \tag{3.10}$$

The solution to Eq. (3.8) satisfying the boundary condition (3.9) can be written as

$$\tilde{G} = A(\alpha, \beta)C(k, z) - \frac{2}{k}e^{i\alpha\xi}e^{i\beta\eta}C(k, z_<)S(k, z_>), \tag{3.11}$$

where

$$z_> = \max(z, \zeta), \tag{3.12}$$

$$z_< = \min(z, \zeta), \tag{3.13}$$

and

$$C(k,z) = \cosh[k(z+H)], \tag{3.14}$$

$$S(k,z) = \sinh[k(z+H)]. \tag{3.15}$$

It may be noticed that the first term on the right-hand side of Eq. (3.11) is the general solution to Eq. (3.8) when the right-hand side is zero, while the second one is a special solution due to the term on the right-hand side of Eq. (3.8).

Taking into account the different conditions in Eqs. (3.2) and (3.3) on $z = 0$, the Wiener-Hopf technique may be used. We first apply the Fourier transform in the x direction to both of them, or

$$\begin{aligned}\widehat{\mathcal{I}}(\alpha,y) = \frac{1}{\sqrt{2\pi}}\int_{-\infty}^{+\infty}\Bigg\{\left[D\nabla^4 - M\left(f - i\varepsilon + iF\frac{\partial}{\partial x}\right)^2 + 1\right]\frac{\partial G}{\partial z} \\ -\left(f - i\varepsilon + iF\frac{\partial}{\partial x}\right)^2 G\Bigg\}_{z=0} e^{i\alpha x}dx,\end{aligned} \tag{3.16}$$

$$\widehat{\mathcal{F}}(\alpha,y) = \frac{1}{\sqrt{2\pi}}\int_{-\infty}^{+\infty}\left[\frac{\partial G}{\partial z} - \left(f - i\varepsilon + iF\frac{\partial}{\partial x}\right)^2 G\right]_{z=0} e^{i\alpha x}dx. \tag{3.17}$$

$\tilde{G}$ in (3.7) is then split into two parts based on the contributions from $y \leqslant 0^-$ and $y \geqslant 0^+$, respectively, or

$$\tilde{G}(\alpha,\beta,z) = \tilde{G}_-(\alpha,\beta,z) + \tilde{G}_+(\alpha,\beta,z), \tag{3.18}$$

where

$$\tilde{G}_\pm(\alpha,\beta,z) = \pm\frac{1}{\sqrt{2\pi}}\int_0^{\pm\infty}\widehat{G}(\alpha,y,z)e^{i\beta y}dy. \tag{3.19}$$

Correspondingly, we write $\tilde{\mathcal{I}}$ and $\tilde{\mathcal{F}}$ as

$$\tilde{\mathcal{I}}(\alpha,\beta) = \tilde{\mathcal{I}}_-(\alpha,\beta) + \tilde{\mathcal{I}}_+(\alpha,\beta), \tag{3.20}$$

$$\tilde{\mathcal{F}}(\alpha,\beta) = \tilde{\mathcal{F}}_-(\alpha,\beta) + \tilde{\mathcal{F}}_+(\alpha,\beta), \tag{3.21}$$

where

$$\tilde{\mathcal{I}}_\pm(\alpha,\beta) = \pm\frac{1}{\sqrt{2\pi}}\int_0^{\pm\infty}\widehat{\mathcal{I}}(\alpha,y)e^{i\beta y}dy, \tag{3.22}$$

and

$$\tilde{\mathcal{F}}_\pm(\alpha,\beta) = \pm\frac{1}{\sqrt{2\pi}}\int_0^{\pm\infty}\widehat{\mathcal{F}}(\alpha,y)e^{i\beta y}dy. \tag{3.23}$$

From Eqs. (3.11), (3.16), and (3.20), we have

$$\begin{aligned}\tilde{\mathcal{I}}(\alpha,\beta) = A(\alpha,\beta)C(k,0)K_i^\varepsilon(\alpha,\beta) - \frac{2}{k}e^{i\alpha\xi}e^{i\beta\eta}C(k,\zeta) \\ \times\{[Dk^4 - M(f - i\varepsilon + \alpha F)^2 + 1]kC(k,0) - (f - i\varepsilon + \alpha F)^2 S(k,0)\},\end{aligned} \tag{3.24}$$

where

$$\begin{aligned}K_i^\varepsilon(\alpha,\beta) &= [Dk^4 - M(f - i\varepsilon + \alpha F)^2 + 1]k\tanh(kH) - (f - i\varepsilon + \alpha F)^2 \\ &\approx K_i(\alpha,\beta) + i\varepsilon\Psi_i(\alpha,\beta),\end{aligned} \tag{3.25}$$

with

$$K_i(\alpha,\beta) = [Dk^4 - M(f+\alpha F)^2 + 1]k\tanh(kH) - (f+\alpha F)^2, \tag{3.26}$$

$$\Psi_i(\alpha,\beta) = 2(f+\alpha F)[Mk\tanh(kH) + 1]. \tag{3.27}$$

Here, $K_i(\alpha,\beta)$ is the dispersion function for a flexural-gravity wave, and $\Psi_i(\alpha,\beta)$ is due to the introduction of $\exp(\varepsilon t)$ with $\varepsilon \to 0^+$. Similarly, from Eqs. (3.11), (3.17), and (3.21), we have

$$\begin{aligned}\tilde{\mathcal{F}}(\alpha,\beta) = A(\alpha,\beta)C(k,0)K_f^{\varepsilon}(\alpha,\beta) - \frac{2}{k}e^{i\alpha\xi}e^{i\beta\eta}C(k,\zeta)\\ \times [kC(k,0) - (f - i\varepsilon + \alpha F)^2 S(k,0)],\end{aligned} \tag{3.28}$$

where

$$\begin{aligned}K_f^{\varepsilon}(\alpha,\beta) &= k\tanh(kH) - (f - i\varepsilon + \alpha F)^2\\ &\approx K_f(\alpha,\beta) + i\varepsilon\Psi_f(\alpha,\beta),\end{aligned} \tag{3.29}$$

with

$$K_f(\alpha,\beta) = k\tanh(kH) - (f+\alpha F)^2, \tag{3.30}$$

$$\Psi_f(\alpha,\beta) = 2(f+\alpha F). \tag{3.31}$$

Here, $K_f(\alpha,\beta)$ is the dispersion function for a free-surface wave. Invoking the boundary conditions (3.2) and (3.3), we have

$$\tilde{\mathcal{I}}_+(\alpha,\beta) = 0 \quad \text{and } \tilde{\mathcal{F}}_-(\alpha,\beta) = 0. \tag{3.32}$$

Eliminating $A(\alpha,\beta)$ from Eqs. (3.24) and (3.28), and using Eqs. (3.20), (3.21), and (3.32), we have

$$\tilde{\mathcal{I}}_-(\alpha,\beta) = \tilde{\mathcal{F}}_+(\alpha,\beta)K(\alpha,\beta) + 2e^{i\alpha\xi}e^{i\beta\eta}\hat{C}(k,\zeta)\frac{J(\alpha,\beta)}{K_f^{\varepsilon}(\alpha,\beta)}, \tag{3.33}$$

where

$$\hat{C}(k,\zeta) = \frac{C(k,\zeta)}{C(k,0)}, \tag{3.34}$$

$$K(\alpha,\beta) = \frac{K_i^{\varepsilon}(\alpha,\beta)}{K_f^{\varepsilon}(\alpha,\beta)}, \tag{3.35}$$

and

$$J(\alpha,\beta) = [Dk^4 - M(f - i\varepsilon + \alpha F)^2](f - i\varepsilon + \alpha F)^2. \tag{3.36}$$

From Eqs. (3.25) and (3.29), the dispersion equations $K_i^{\varepsilon}(\alpha,\beta) = 0$ and $K_f^{\varepsilon}(\alpha,\beta) = 0$ with $\varepsilon \to 0^+$ give the wave propagation properties in the ice-covered region and free-surface region, respectively. From (3.26) at a given α, $K_i(\alpha,\beta) = 0$ has two real roots: $k = \pm\kappa_0$ ($\kappa_0 > 0$), four complex roots: $k = \pm\kappa_{-2}$ and $k = \pm\kappa_{-1}$ (κ_{-1} is located in the first quadrant and $\kappa_{-1} = -\bar{\kappa}_{-2}$ with the overbar denoting the complex conjugate), and an infinite number of imaginary roots: $k = \pm\kappa_m$ [$\mathrm{Im}(\kappa_m) > 0$ and $m = 1,\ldots,\infty$]. From Appendix A, we can see that corresponding to $K_i(\alpha,\beta) = 0$ at $k = \kappa_0$, $K_i^{\varepsilon}(\alpha,\beta) = 0$ at $k = \kappa_0 - i\varepsilon_1\mathrm{sgn}(f+\alpha F)$, where $\varepsilon_1 \to 0^+$. Then, the roots of the dispersion equation $K_i^{\varepsilon}(\alpha,\beta) = 0$ for β can be written as χ_m with

$$\chi_m = \pm\sqrt{\kappa_m^2 - \alpha^2}\,(0 \leqslant \arg(\chi_m) \leqslant \pi). \tag{3.37}$$

It should be noticed that the sign before the square root should be taken to ensure $0 \leqslant \arg(\chi_m) \leqslant \pi$. Based on this condition, when $\kappa_0 > |\alpha|$, we take $\chi_0 = -\mathrm{sgn}(f+\alpha F)\sqrt{\kappa_0^2 - \alpha^2} + i\varepsilon_2$, where

$\varepsilon_2 \to 0^+$. Similarly, the dispersion equation $K_f(\alpha, \beta) = 0$ from Eq. (3.30) at a given α has two real roots: $k = \pm k_0$ ($k_0 > 0$), and an infinite number of imaginary roots: $k = \pm k_m$ [$\mathrm{Im}(k_m) > 0$ and $m = 1, \ldots, \infty$]. Corresponding to $K_f(\alpha, \beta) = 0$ at $k = k_0$, $K_f^\varepsilon(\alpha, \beta) = 0$ at $k = k_0 - i\varepsilon_3 \mathrm{sgn}(f + \alpha F)$, where $\varepsilon_3 \to 0^+$. Thus, the roots of the dispersion equation $K_f^\varepsilon(\alpha, \beta) = 0$ for β can be written as γ_m with

$$\gamma_m = \pm\sqrt{k_m^2 - \alpha^2} \quad (0 \leqslant \arg(\gamma_m) \leqslant \pi), \tag{3.38}$$

where the sign $\pm$ will be chosen based on the condition of $0 \leqslant \arg(\gamma_m) \leqslant \pi$. Noticing $\arg[k_0 - i\varepsilon_3 \mathrm{sgn}(f + \alpha F)]$ is taken within $[0, 2\pi)$, when $k_0 > |\alpha|$, we then have $\gamma_0 = -\mathrm{sgn}(f + \alpha F)\sqrt{k_0^2 - \alpha^2} + i\varepsilon_4$, where $\varepsilon_4 \to 0^+$.

When $y \leqslant 0^-$, where the upper boundary is a free surface, $\widehat{G}$ can be written in the form of vertical mode expansion as

$$\widehat{G} = \sum_{m=0}^{\infty} a_m e^{-i\gamma_m y} \frac{\cosh[k_m(z + H)]}{\cosh(k_m H)}. \tag{3.39}$$

Based on the definition of γ_m, this gives an outgoing wave at $y \to -\infty$. Substituting this into Eq. (3.19), we have that $\tilde{G}_-$ is analytic when $\mathrm{Im}(\beta) < \tau_1$. Here, $\tau_1 = \min[\mathrm{Im}(\gamma_1), \mathrm{Im}(\gamma_0)] > 0$, which is equal to ε_4 when $k_0 > |\alpha|$. Similarly, from Eq. (3.37), for $y \geqslant 0^+$, where the upper water boundary is covered by the ice sheet, we may write $\widehat{G}$ as

$$\widehat{G} = \sum_{m=-2}^{\infty} b_m e^{i\chi_m y} \frac{\cosh[\kappa_m(z + H)]}{\cosh(\kappa_m H)}. \tag{3.40}$$

This, with Eq. (3.19), indicates that $\tilde{G}_+$ is analytic when $\mathrm{Im}(\beta) > -\tau_2$. Here, $\tau_2 = \min[\mathrm{Im}(\chi_1), \mathrm{Im}(\chi_0)] > 0$, which is equal to ε_2 when $\kappa_0 \geqslant |\alpha|$.

In accordance with the Wiener-Hopf technique, at a given α, we need to factorize the function $K(\alpha, \beta)$ as

$$K(\alpha, \beta) = K_-(\alpha, \beta) K_+(\alpha, \beta), \tag{3.41}$$

based on the regions in the β plane, where $K_-(\alpha, \beta)$ and $K_+(\alpha, \beta)$ are analytical in their own regions, respectively. From Appendix B, we have

$$K_\pm(\alpha, \beta) = \frac{(\beta \pm \chi_{-2})(\beta \pm \chi_{-1})}{\kappa_{-2}\kappa_{-1}} \prod_{m=0}^{\infty} \frac{k_m(\beta \pm \chi_m)}{\kappa_m(\beta \pm \gamma_m)}, \tag{3.42}$$

where $K_\pm$ have zeros at all the roots of the dispersion relation $K_i^\varepsilon(\alpha, \beta) = 0$, and poles at all the roots of the dispersion relation $K_f^\varepsilon(\alpha, \beta) = 0$. We define the region S_+ as $\mathrm{Im}(\beta) > -\bar{\tau}$ and the region S_- as $\mathrm{Im}(\beta) < \bar{\tau}$, where $\bar{\tau} = \min(\tau_1, \tau_2)$ with τ_1 and τ_2 defined below Eqs. (3.39) and (3.40), respectively. Then, in the region S_+ (S_-), K_+ (K_-) is analytical, and also K_+ (K_-) has no zero.

Substituting Eq. (3.41) into Eq. (3.33), we have

$$\tilde{\mathcal{F}}_+(\alpha, \beta) K_+(\alpha, \beta) = \frac{\tilde{\mathcal{I}}_-(\alpha, \beta)}{K_-(\alpha, \beta)} - 2e^{i\alpha\xi} e^{i\beta\eta} \hat{C}(k, \zeta) J(\alpha, \beta) \frac{K_+(\alpha, \beta)}{K_i^\varepsilon(\alpha, \beta)}, \tag{3.43}$$

the last term of which needs to be further decomposed. We have

$$e^{i\beta\eta} \hat{C}(k, \zeta) J(\alpha, \beta) \frac{K_+(\alpha, \beta)}{K_i^\varepsilon(\alpha, \beta)} = M_+(\alpha, \beta) + M_-(\alpha, \beta), \tag{3.44}$$

where M_+ (M_-) is analytical in S_+ (S_-). When $\eta < 0$, we may use the Cauchy integral [37] in the lower half plane and obtain M_+ as

$$M_+(\alpha,\beta) = \sum_{m=0}^{\infty} \frac{e^{-i\gamma_m\eta}\hat{C}(k_m,\zeta)J(\alpha,-\gamma_m)}{K_-(\alpha,-\gamma_m)K_f^{\varepsilon\prime}(\alpha,-\gamma_m)(\beta+\gamma_m)}. \tag{3.45}$$

Subsequently, M_- can be obtained from

$$M_-(\alpha,\beta) = \frac{e^{i\beta\eta}\hat{C}(k,\zeta)J(\alpha,\beta)}{K_-(\alpha,\beta)K_f^{\varepsilon}(\alpha,\beta)} - M_+(\alpha,\beta). \tag{3.46}$$

When $\eta > 0$, Cauchy integral can be applied in the upper half plane to obtain M_-. Here, Eq. (3.41) has been used, and

$$K_f^{\varepsilon\prime}(\alpha,\beta) = \frac{\partial K_f^{\varepsilon}(\alpha,\beta)}{\partial\beta}. \tag{3.47}$$

Substituting Eq. (3.44) into Eq. (3.43), we have

$$\tilde{\mathcal{F}}_+(\alpha,\beta)K_+(\alpha,\beta) + 2e^{i\alpha\xi}M_+(\alpha,\beta) = \frac{\tilde{\mathcal{I}}_-(\alpha,\beta)}{K_-(\alpha,\beta)} - 2e^{i\alpha\xi}M_-(\alpha,\beta). \tag{3.48}$$

Each term on the left-hand side of Eq. (3.48) is analytical in the region S_+, while that on the right-hand side is analytical in the region S_-. Both of them are analytical in the overlapping region of S_+ and S_-, or $-\bar{\tau} < \mathrm{Im}(\beta) < \bar{\tau}$. Through analytical continuation, Eq. (3.48) defines a function $Q(\beta)$, which is analytical in the whole β plane. As $Q(\beta)$ is an entire function, it can be written as a power series. Then, we may rewrite Eq. (3.48) as

$$Q(\beta) = \tilde{\mathcal{F}}_+(\alpha,\beta)K_+(\alpha,\beta) + 2e^{i\alpha\xi}M_+(\alpha,\beta) = \frac{\tilde{\mathcal{I}}_-(\alpha,\beta)}{K_-(\alpha,\beta)} - 2e^{i\alpha\xi}M_-(\alpha,\beta). \tag{3.49}$$

Replacing $\tilde{\mathcal{I}}_-(\alpha,\beta)$ in Eq. (3.24) by Eq. (3.49), and noticing Eqs. (3.20) and (3.32), we have

$$\begin{aligned} A(\alpha,\beta) = {} & \frac{Q(\beta)K_-(\alpha,\beta)}{C(k,0)K_i^{\varepsilon}(\alpha,\beta)} + 2e^{i\alpha\xi}\frac{M_-(\alpha,\beta)K_-(\alpha,\beta)}{C(k,0)K_i^{\varepsilon}(\alpha,\beta)} \\ & + 2e^{i\alpha\xi}e^{i\beta\eta}\hat{C}(k,\zeta)\left[\frac{Dk^4 - M(f - i\varepsilon + \alpha F)^2 + 1}{C(k,0)K_i^{\varepsilon}(\alpha,\beta)} + \frac{S(k,0)}{k}\right]. \end{aligned} \tag{3.50}$$

Similarly, replacing $\tilde{\mathcal{F}}_+(\alpha,\beta)$ in Eq. (3.28) by Eq. (3.49), we obtain

$$\begin{aligned} A(\alpha,\beta) = {} & \frac{Q(\beta)}{C(k,0)K_+(\alpha,\beta)K_f^{\varepsilon}(\alpha,\beta)} - 2e^{i\alpha\xi}\frac{M_+(\alpha,\beta)}{C(k,0)K_+(\alpha,\beta)K_f^{\varepsilon}(\alpha,\beta)} \\ & + 2e^{i\alpha\xi}e^{i\beta\eta}\hat{C}(k,\zeta)\left[\frac{1}{C(k,0)K_f^{\varepsilon}(\alpha,\beta)} + \frac{S(k,0)}{k}\right]. \end{aligned} \tag{3.51}$$

Substituting Eq. (3.50) into (3.11), we have

$$\tilde{G} = \tilde{G}_I + \hat{C}(k,z)\frac{Q(\beta)K_-(\alpha,\beta)}{K_i^{\varepsilon}(\alpha,\beta)} + 2e^{i\alpha\xi}\hat{C}(k,z)\frac{M_-(\alpha,\beta)K_-(\alpha,\beta)}{K_i^{\varepsilon}(\alpha,\beta)}. \tag{3.52}$$

Here, $\tilde{G}_I$ is given in Eq. (D3), which is the double Fourier transform of the Green function G_I for the case of water surface being fully covered by an ice sheet of infinite extent. Applying the inverse Fourier transform to Eq. (3.52) with respect to β, or

$$\hat{G}(\alpha,y,z) = \frac{1}{\sqrt{2\pi}}\int_{-\infty}^{+\infty}\tilde{G}(\alpha,\beta,z)e^{-i\beta y}d\beta, \tag{3.53}$$

we have

$$\widehat{G} = \widehat{G}_I + \frac{1}{\sqrt{2\pi}} \int_{-\infty}^{+\infty} e^{-i\beta y} \hat{C}(k, z) \frac{Q(\beta) K_-(\alpha, \beta)}{K_i^\varepsilon(\alpha, \beta)} d\beta + \frac{2e^{i\alpha\xi}}{\sqrt{2\pi}} \int_{-\infty}^{+\infty} e^{-i\beta y} \hat{C}(k, z) \frac{M_-(\alpha, \beta) K_-(\alpha, \beta)}{K_i^\varepsilon(\alpha, \beta)} d\beta, \tag{3.54}$$

where $\widehat{G}_I$ is given in Eq. (D7). Because χ_m and γ_m both tend to $im\pi$ as $m \to \infty$, from Eqs. (3.25) and (3.42), we have that $K_i^\varepsilon(\alpha, \beta) = O(\beta^5)$ and $K_-(\alpha, \beta) = O(\beta^2)$ when $\beta \to \infty$. Thus, in Eq. (3.54), we may write

$$Q(\beta) = 2e^{i\alpha\xi}[a(\alpha) + b(\alpha)\beta], \tag{3.55}$$

as β^2 in $Q(\beta)$ would lead to a singularity in the form of $\ln(\sqrt{y^2 + z^2})$ near the edge of the ice sheet, and β^n with $n > 2$ would lead to a higher-order singularity in the form of $d^{n-2}[\ln(\sqrt{y^2 + z^2})]/dy^{n-2}$ or $d^{n-2}[\ln(\sqrt{y^2 + z^2})]/dz^{n-2}$.

From Eq. (3.54), we obtain

$$\left(\frac{\partial \widehat{G}}{\partial z}\right)_{z=0} = \frac{2e^{i\alpha\xi}}{\sqrt{2\pi}} [\widehat{I}_1(\alpha, y) a(\alpha) + \widehat{I}_2(\alpha, y) b(\alpha) + \widehat{I}_3(\alpha, y)], \tag{3.56}$$

where

$$\widehat{I}_1(\alpha, y) = \int_{-\infty}^{+\infty} e^{-i\beta y} k \tanh(kH) \frac{K_-(\alpha, \beta)}{K_i^\varepsilon(\alpha, \beta)} d\beta, \tag{3.57}$$

$$\widehat{I}_2(\alpha, y) = \int_{-\infty}^{+\infty} e^{-i\beta y} \beta k \tanh(kH) \frac{K_-(\alpha, \beta)}{K_i^\varepsilon(\alpha, \beta)} d\beta, \tag{3.58}$$

$$\widehat{I}_3(\alpha, y) = \int_{-\infty}^{+\infty} e^{-i\beta y} \left[k \tanh(kH) \frac{M_-(\alpha, \beta) K_-(\alpha, \beta)}{K_i^\varepsilon(\alpha, \beta)} + e^{i\beta\eta} \hat{C}(k, \zeta) \frac{(f - i\varepsilon + \alpha F)^2}{K_i^\varepsilon(\alpha, \beta)} \right] d\beta. \tag{3.59}$$

In Eq. (3.59), the following equation has been used:

$$\left.\frac{\partial \widehat{G}_I}{\partial z}\right|_{z=0} = \frac{2e^{i\alpha\xi}}{\sqrt{2\pi}} \int_{-\infty}^{+\infty} e^{i\beta(\eta - y)} \hat{C}(k, \zeta) \frac{(f - i\varepsilon + \alpha F)^2}{K_i^\varepsilon(\alpha, \beta)} d\beta. \tag{3.60}$$

Applying Fourier transform to the ice-edge condition (3.4) with respect to x, we have

$$\widehat{\mathcal{B}}\left(\frac{\partial \widehat{G}}{\partial z}\right) = 0 \quad \text{and } \widehat{\mathcal{S}}\left(\frac{\partial \widehat{G}}{\partial z}\right) = 0 \quad (y = 0^+ \text{ and } z = 0), \tag{3.61}$$

where

$$\widehat{\mathcal{B}} = \frac{\partial^2}{\partial y^2} - \nu\alpha^2, \tag{3.62}$$

$$\widehat{\mathcal{S}} = \frac{\partial}{\partial y}\left[\frac{\partial^2}{\partial y^2} - (2 - \nu)\alpha^2\right]. \tag{3.63}$$

Substituting Eq. (3.56) into (3.61), we have

$$\begin{bmatrix} W_{11} & W_{12} \\ W_{21} & W_{22} \end{bmatrix} \begin{Bmatrix} a(\alpha) \\ b(\alpha) \end{Bmatrix} = \begin{Bmatrix} D_1 \\ D_2 \end{Bmatrix}, \tag{3.64}$$

where

$$W_{11} = \widehat{I}_1''(\alpha, 0) - \nu\alpha^2 \widehat{I}_1(\alpha, 0), \tag{3.65}$$

$$W_{12} = \widehat{I}_2''(\alpha, 0) - \nu\alpha^2 \widehat{I}_2(\alpha, 0), \tag{3.66}$$

$$W_{21} = \widehat{I}_1'''(\alpha, 0) - (2-\nu)\alpha^2 \widehat{I}_1'(\alpha, 0), \tag{3.67}$$

$$W_{22} = \widehat{I}_2'''(\alpha, 0) - (2-\nu)\alpha^2 \widehat{I}_2'(\alpha, 0), \tag{3.68}$$

$$D_1 = \nu\alpha^2 \widehat{I}_3(\alpha, 0) - \widehat{I}_3''(\alpha, 0), \tag{3.69}$$

$$D_2 = (2-\nu)\alpha^2 \widehat{I}_3'(\alpha, 0) - \widehat{I}_3'''(\alpha, 0). \tag{3.70}$$

Here, the prime denotes partial derivative with respect to y. The computation of Eqs. (3.65) to (3.70) is given in Appendix C.

Substituting Eq. (3.55) into Eq. (3.54) and performing the inverse transform with respect to α, we have

$$G = G_I + G_{IF} + G_{IE}, \tag{3.71}$$

where G_I is given in Eq. (D8), and

$$G_{IF} = \frac{1}{\pi}\int_{-\infty}^{+\infty}\int_{-\infty}^{+\infty} e^{i[\alpha(\xi-x)-\beta y]}\hat{C}(k,z)\frac{M_-(\alpha,\beta)K_-(\alpha,\beta)}{K_i^{\varepsilon}(\alpha,\beta)}d\alpha d\beta, \tag{3.72}$$

$$G_{IE} = \frac{1}{\pi}\int_{-\infty}^{+\infty}\int_{-\infty}^{+\infty} e^{i[\alpha(\xi-x)-\beta y]}\hat{C}(k,z)[a(\alpha)+b(\alpha)\beta]\frac{K_-(\alpha,\beta)}{K_i^{\varepsilon}(\alpha,\beta)}d\alpha d\beta. \tag{3.73}$$

Equation (3.71) may be rewritten in another form. Substituting Eq. (3.51) into Eq. (3.11), and using Eq. (3.55), we have

$$\tilde{G} = \tilde{G}_F + 2e^{i\alpha\xi}\hat{C}(k,z)\frac{a(\alpha)+b(\alpha)\beta}{K_+(\alpha,\beta)K_f^{\varepsilon}(\alpha,\beta)} - 2e^{i\alpha\xi}\hat{C}(k,z)\frac{M_+(\alpha,\beta)}{K_+(\alpha,\beta)K_f^{\varepsilon}(\alpha,\beta)}, \tag{3.74}$$

where $\tilde{G}_F$ is given in Eq. (D12). Taking inverse Fourier transform of Eq. (3.74) with respect to α and β, we have

$$G = G_F + G_{FI} + G_{FE}, \tag{3.75}$$

where G_F is the free-surface Green function given in Eq. (D10), and

$$G_{FI} = -\frac{1}{\pi}\int_{-\infty}^{+\infty}\int_{-\infty}^{+\infty} e^{i[\alpha(\xi-x)-\beta y]}\hat{C}(k,z)\frac{M_+(\alpha,\beta)}{K_+(\alpha,\beta)K_f^{\varepsilon}(\alpha,\beta)}d\alpha d\beta, \tag{3.76}$$

$$G_{FE} = \frac{1}{\pi}\int_{-\infty}^{+\infty}\int_{-\infty}^{+\infty} e^{i[\alpha(\xi-x)-\beta y]}\hat{C}(k,z)\frac{a(\alpha)+b(\alpha)\beta}{K_+(\alpha,\beta)K_f^{\varepsilon}(\alpha,\beta)}d\alpha d\beta. \tag{3.77}$$

Equations (3.35) and (3.41) indicate that $G_{FE} = G_{IE}$.

For the free-surface Green function, the wave amplitude at the track is unbounded when both the source point and field point are on the water surface, or $y = \eta$ and $z = \zeta = 0$ [38]. This is a result of idealization of the mathematical model and is nonphysical. It can be eliminated through the inclusion of fluid viscosity effects as shown in Ref. [39]. Here, while rigorous derivation would be required to make a solid conclusion, similar behavior is also expected.

IV. WAVE PATTERNS INDUCED BY THE POINT SOURCE

A. Ice-sheet deflection wave pattern

We use Eq. (3.71) to analyze the wave patterns in the domain covered by a semi-infinite ice sheet or $y \geqslant 0^+$. Invoking the kinematic boundary condition on the ice sheet, or

$$\left[i(f - i\varepsilon) - F\frac{\partial}{\partial x}\right]W = \frac{\partial G}{\partial z} \quad (z = 0), \tag{4.1}$$

where W is the deflection of the ice sheet, and using Fourier transform, we have

$$W = \frac{1}{\sqrt{2\pi}}\int_{-\infty}^{+\infty}\frac{e^{-i\alpha x}}{i(f - i\varepsilon + \alpha F)}\left(\frac{\partial \widehat{G}}{\partial z}\right)_{z=0} d\alpha. \tag{4.2}$$

Invoking Eq. (3.56), we obtain

$$W = W_I + W_{IF} + W_{IE}, \tag{4.3}$$

where

$$W_I = \frac{1}{i\pi}\int_{-\infty}^{+\infty}(f - i\varepsilon + \alpha F)e^{i\alpha(\xi - x)}d\alpha\int_{-\infty}^{+\infty}e^{i\beta(\eta - y)}\frac{\hat{C}(k,\zeta)}{K_i^{\varepsilon}(\alpha,\beta)}d\beta, \tag{4.4}$$

$$W_{IF} = \frac{1}{i\pi}\int_{-\infty}^{+\infty}\frac{e^{i\alpha(\xi - x)}}{f - i\varepsilon + \alpha F}d\alpha\int_{-\infty}^{+\infty}e^{-i\beta y}k\tanh(kH)\frac{M_-(\alpha,\beta)K_-(\alpha,\beta)}{K_i^{\varepsilon}(\alpha,\beta)}d\beta, \tag{4.5}$$

$$W_{IE} = \frac{1}{i\pi}\int_{-\infty}^{+\infty}\frac{e^{i\alpha(\xi - x)}}{f - i\varepsilon + \alpha F}d\alpha\int_{-\infty}^{+\infty}e^{-i\beta y}k\tanh(kH)[a(\alpha) + b(\alpha)\beta]\frac{K_-(\alpha,\beta)}{K_i^{\varepsilon}(\alpha,\beta)}d\beta. \tag{4.6}$$

For integration with respect to β, we may use the Cauchy residual theorem in the lower half of the complex β plane, as the integration along an infinitely large semicircle is zero. Taking into account of all the poles of $K_i(\alpha,\beta) = 0$, Eqs. (4.4) and (4.6) become

$$W_I = -2\int_{-\infty}^{+\infty}(f + \alpha F)e^{i\alpha(\xi - x)}\sum_{m=-2}^{\infty}e^{i\chi_m(y-\eta)}\frac{\hat{C}(\kappa_m,\zeta)}{K'_i(\alpha,-\chi_m)}d\alpha, \tag{4.7}$$

$$W_{IE} = -2\int_{-\infty}^{+\infty}e^{i\alpha(\xi - x)}\sum_{m=-2}^{\infty}e^{i\chi_m y}\kappa_m\tanh(\kappa_m H)\frac{a(\alpha) - b(\alpha)\chi_m}{f + \alpha F}\frac{K_-(\alpha,-\chi_m)}{K'_i(\alpha,-\chi_m)}d\alpha. \tag{4.8}$$

Substituting Eq. (3.46) into Eq. (4.5), we have

$$W_{IF} = \frac{1}{i\pi}\int_{-\infty}^{+\infty}\frac{e^{i\alpha(\xi - x)}}{f - i\varepsilon + \alpha F}d\alpha\int_{-\infty}^{+\infty}\frac{e^{-i\beta y}k\tanh(kH)}{K_i^{\varepsilon}(\alpha,\beta)}$$
$$\times\left[\frac{e^{i\beta\eta}\hat{C}(k,\zeta)J(\alpha,\beta)}{K_f^{\varepsilon}(\alpha,\beta)} - K_-(\alpha,\beta)\sum_{m=0}^{\infty}\frac{e^{-i\gamma_m\eta}\hat{C}(k_m,\zeta)J(\alpha,-\gamma_m)}{K_-(\alpha,-\gamma_m)K_f^{\varepsilon\prime}(\alpha,-\gamma_m)(\beta + \gamma_m)}\right]d\beta, \tag{4.9}$$

which can be converted to a series as

$$W_{IF} = 2\int_{-\infty}^{+\infty}\frac{e^{i\alpha(\xi - x)}}{f + \alpha F}\sum_{m=-2}^{\infty}\frac{e^{i\chi_m y}}{K'_i(\alpha,-\chi_m)}\left[(f + \alpha F)^2 e^{-i\chi_m\eta}\hat{C}(\kappa_m,\zeta)\right.$$
$$\left. + \kappa_m\tanh(\kappa_m H)K_-(\alpha,-\chi_m)\sum_{j=0}^{\infty}\frac{e^{-i\gamma_j\eta}\hat{C}(k_j,\zeta)J(\alpha,-\gamma_j)}{K_-(\alpha,-\gamma_j)K'_f(\alpha,-\gamma_j)(\gamma_j - \chi_m)}\right]d\alpha, \tag{4.10}$$

where Eq. (C5) has been used.

B. Free-surface wave pattern

Here, we shall use Eq. (3.75) to analyze the free-surface wave pattern in the region of $y \leqslant 0^-$. Applying the inverse Fourier transform to Eq. (3.74) with respect to β, and substituting the obtained results into Eq. (4.2), we have

$$W = W_F + W_{FI} + W_{FE}, \tag{4.11}$$

where

$$W_F = \frac{1}{i\pi}\int_{-\infty}^{+\infty}(f - i\varepsilon + \alpha F)e^{i\alpha(\xi - x)}d\alpha \int_{-\infty}^{+\infty} e^{i\beta(\eta - y)}\frac{\hat{C}(k,\zeta)}{K_f^{\varepsilon}(\alpha,\beta)}d\beta, \tag{4.12}$$

$$W_{FI} = -\frac{1}{i\pi}\int_{-\infty}^{+\infty}\frac{e^{i\alpha(\xi - x)}}{f - i\varepsilon + \alpha F}d\alpha \int_{-\infty}^{+\infty} e^{-i\beta y}k\tanh(kH)\frac{M_+(\alpha,\beta)}{K_+(\alpha,\beta)K_f^{\varepsilon}(\alpha,\beta)}d\beta, \tag{4.13}$$

$$W_{FE} = \frac{1}{i\pi}\int_{-\infty}^{+\infty}\frac{e^{i\alpha(\xi - x)}}{f - i\varepsilon + \alpha F}d\alpha \int_{-\infty}^{+\infty} e^{-i\beta y}k\tanh(kH)\frac{a(\alpha) + b(\alpha)\beta}{K_+(\alpha,\beta)K_f^{\varepsilon}(\alpha,\beta)}d\beta. \tag{4.14}$$

Here, Eqs. (3.35) and (3.41) indicate that $W_{FE} = W_{IE}$. Similar to the ice-sheet deflection wave, the integrals with respect to β in the above equations can be converted into a series using the Cauchy residual theorem in the upper half plane. For Eqs. (4.12) and (4.14), we have

$$W_F = 2\int_{-\infty}^{+\infty}(f + \alpha F)e^{i\alpha(\xi - x)}\sum_{m=0}^{\infty} e^{i\gamma_m|\eta - y|}\frac{\hat{C}(k_m,\zeta)}{K'_f(\alpha,\gamma_m)}d\alpha, \tag{4.15}$$

$$W_{FE} = 2\int_{-\infty}^{+\infty}(f + \alpha F)e^{i\alpha(\xi - x)}\sum_{m=0}^{\infty} e^{-i\gamma_m y}\frac{a(\alpha) + b(\alpha)\gamma_m}{K_+(\alpha,\gamma_m)K'_f(\alpha,\gamma_m)}d\alpha, \tag{4.16}$$

where $k_m\tanh(k_mH) = (f + \alpha F)^2$ has been used. Substituting Eq. (3.45) into Eq. (4.13), we have

$$W_{FI} = -\frac{1}{i\pi}\int_{-\infty}^{+\infty}\int_{-\infty}^{+\infty}\frac{e^{i\alpha(\xi - x)}}{f - i\varepsilon + \alpha F}\times\frac{e^{-i\beta y}k\tanh(kH)}{K_+(\alpha,\beta)K_f^{\varepsilon}(\alpha,\beta)}$$
$$\times\sum_{m=0}^{\infty}\frac{e^{-i\gamma_m\eta}\hat{C}(k_m,\zeta)J(\alpha,-\gamma_m)}{K_-(\alpha,-\gamma_m)K_f^{\varepsilon\prime}(\alpha,-\gamma_m)(\beta + \gamma_m)}d\alpha d\beta, \tag{4.17}$$

which can be converted to a series as

$$W_{FI} = -2\int_{-\infty}^{+\infty}e^{i\alpha(\xi - x)}\sum_{m=0}^{\infty}\frac{e^{-i\gamma_m y}(f + \alpha F)}{K_+(\alpha,\gamma_m)K'_f(\alpha,\gamma_m)}\sum_{j=0}^{\infty}\frac{e^{-i\gamma_j\eta}\hat{C}(k_j,\zeta)J(\alpha,-\gamma_j)}{K_-(\alpha,-\gamma_j)K'_f(\alpha,-\gamma_j)(\gamma_m + \gamma_j)}d\alpha. \tag{4.18}$$

V. NUMERICAL RESULTS

To provide meaningful results in physics, the typical values of the parameters of ice sheet and fluid are set to be

$$E = 5\ \text{GPa},\quad \nu = 0.3,\quad \rho_i = 922.5\ \text{kg/m}^3,\quad \rho_w = 1025\ \text{kg/m}^3,\quad H = 100\ \text{m}, \tag{5.1}$$

which are similar to those obtained from the field experiment in polar regions [40]. As given in Eq. (3.1), all the results in the following text will be provided in the dimensionless form, based on the combination of the density of water ρ_w, the acceleration due to gravity $g = 9.8\ \text{m/s}^2$, and a characteristic ship length $l = 100$ m. The forward speed U will vary from 0 to $1.1\sqrt{gl}$ m/s, which includes the typical range of a displacement ship and a high-speed air-cushion vehicle [41]. The range of radian frequency ω is set to be from 0 to $4\sqrt{g/l}$ rad/s [42].

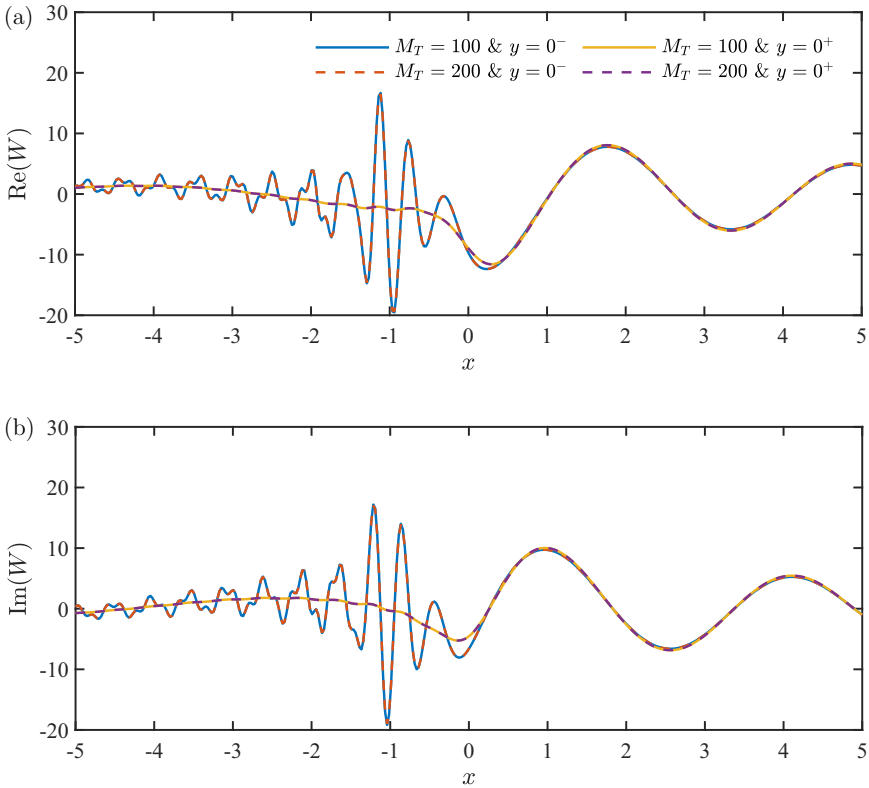

FIG. 2. The free-surface wave elevation at $y = 0^-$ and ice-sheet deflection at $y = 0^+$, with different truncated number M_T. (a) real part of W; (b) imaginary part of W $[(\xi, \eta, \zeta) = (0, -0.5, -0.1)$, $F = 0.2$, $f = 1$, $h = 0.01$, $D = 4.5582 \times 10^{-4}$, $M = 9 \times 10^{-3}]$.

Numerical computations of $a(\alpha)$ and $b(\alpha)$ in Eq. (3.64) are carried out through truncating the infinite summations in Appendix B at a finite number of $m = M_T$. The same number $m = M_T$ is also used for the calculation of $K_\pm$ and $M_\pm$ in Eqs. (3.42), (3.45), and (3.46). Similar to the numerical scheme in Milinazzo *et al.* [30], the ice-sheet deflection in Sec. IV A and free-surface wave elevation in Sec. IV B are calculated numerically using an adaptive Gaussian quadrature, in which the truncated terms of the infinite summations depend on the value of y. Five-decimal accuracy is used to decide whether the convergence is obtained.

A. Convergence study and verification

Computations are first carried out for the waves near the ice edge induced by a source at $(\xi, \eta, \zeta) = (0, -0.5, -0.1)$. Figure 2 shows the free-surface wave elevation at $y = 0^-$ and ice-sheet deflection at $y = 0^+$. The Froude number is taken to be $F = 0.2$, and the radian frequency of oscillation is set to be $f = 1$. It can be observed that there is no visible difference between the results obtained by $M_T = 100$ and $M_T = 200$, which indicates that the convergence has been achieved. In the following texts, the former will be used to carry out the numerical computations of the results, if it is not specified.

Further verifications are carried out for a special case with $F = 0$. The Green function for a source oscillating without forward speed has been derived by Li and Wu [24], through first applying the Fourier transform in the longitudinal direction along the ice edge, and then using the MEE in the transverse plane normal to the ice edge. Figure 3 shows the free-surface wave elevation at $y = 0^-$ and ice-sheet deflection at $y = 0^+$. The position of the source point is the same as that in Fig. 1, and

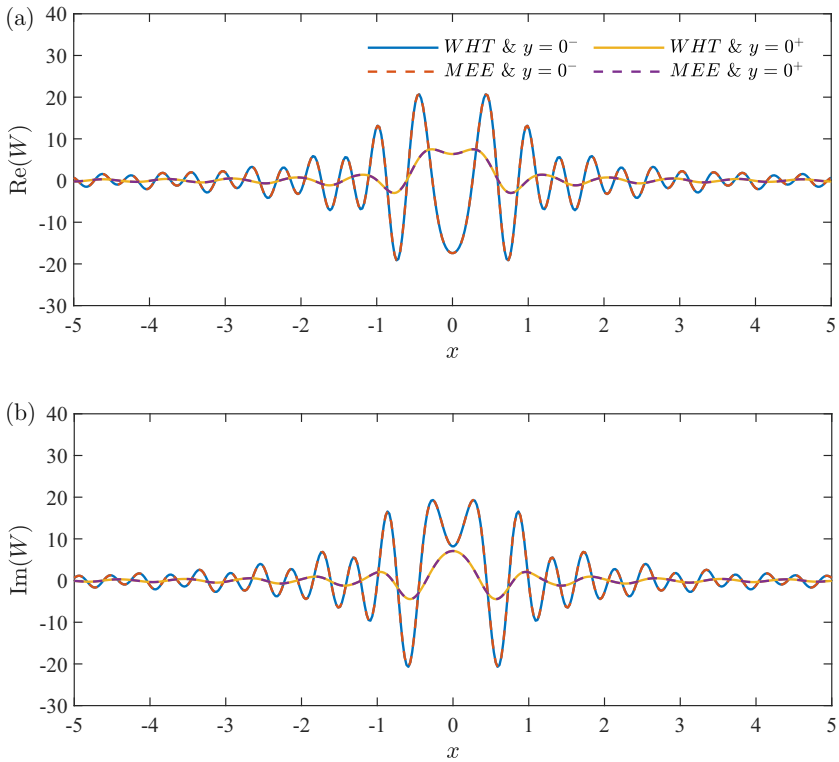

FIG. 3. The free-surface wave elevation at $y = 0^-$ and ice-sheet deflection at $y = 0^+$, computed through different methods. (a) Real part of W; (b) imaginary part of W $[(\xi, \eta, \zeta) = (0, -0.5, -0.1), F = 0, f = 4, h = 0.01, D = 4.5582 \times 10^{-4}, M = 9 \times 10^{-3}]$.

$f = 4$. It can be seen from this figure that the results obtained by the WHT show a good agreement with those computed by the MEE. As noted by Evans and Porter [43], the eigenfunctions for the vertical modes of flexural gravity wave motion are nonorthogonal in a standard sense, and could be incomplete. To validate the method of MEE, they solved the same two-dimensional diffraction problem by an ice crack through the Green function approach, and showed that the two solutions are identical. Similar verifications were performed by Brocklehurst *et al.* [44] and Korobkin *et al.* [45] through the linear diffraction problem for a vertical circular cylinder frozen in an ice sheet of infinite extent, and found that the Weber integral transform and the MEE gave identical results. Here, as demonstrated in Fig. 3, the WHT and MEE give the same numerical results for the upper water surface partially covered by an ice sheet.

B. Wave motions along the ice edge

The free-surface wave elevation and ice-sheet deflection is generally different at the ice edge, as shown in Figs. 2 and 3. This is because that although they share the same kinematic boundary condition (2.6), the dynamic boundary condition is different. Substituting Eq. (3.46) into Eq. (4.5), we have

$$W_{IF} = \frac{1}{i\pi}\int_{-\infty}^{+\infty}(f - i\varepsilon + \alpha F)e^{i\alpha(\xi - x)}d\alpha \int_{-\infty}^{+\infty} e^{i\beta(\eta - y)}\hat{C}(k, \zeta)\frac{K_i^{\varepsilon}(\alpha, \beta) - K_f^{\varepsilon}(\alpha, \beta)}{K_i^{\varepsilon}(\alpha, \beta)K_f^{\varepsilon}(\alpha, \beta)}d\beta$$
$$- \frac{1}{i\pi}\int_{-\infty}^{+\infty}\frac{e^{i\alpha(\xi - x)}}{f - i\varepsilon + \alpha F}d\alpha \int_{-\infty}^{+\infty} e^{-i\beta y}k\tanh(kH)\frac{M_+(\alpha, \beta)}{K_+(\alpha, \beta)K_f^{\varepsilon}(\alpha, \beta)}d\beta. \tag{5.2}$$

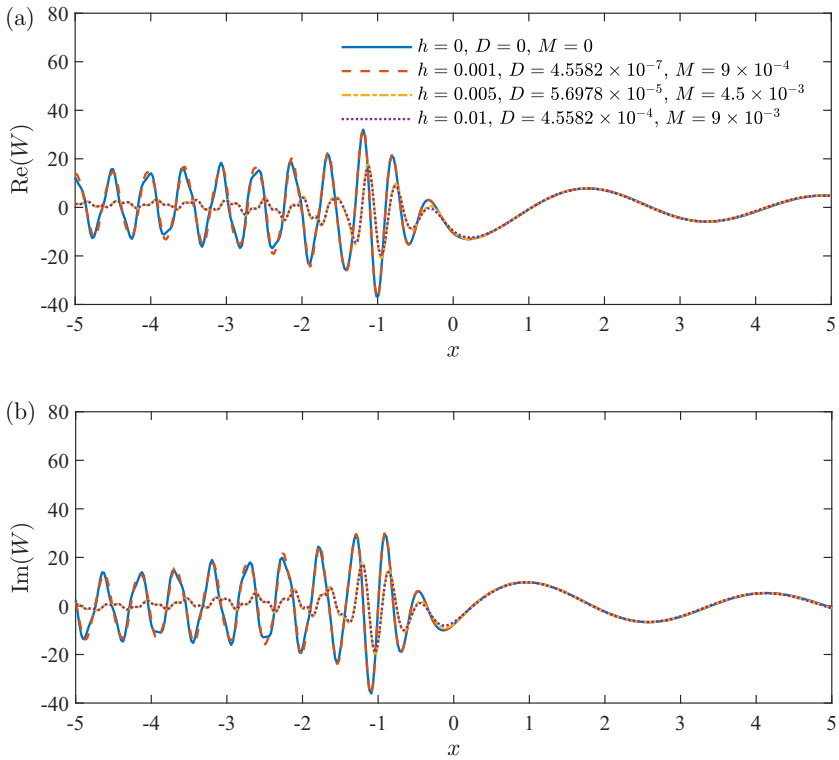

FIG. 4. The free-surface wave elevation W at $y = 0^-$, with different ice thickness h. (a) Real part of W; (b) imaginary part of W $[(\xi, \eta, \zeta) = (0, -0.5, -0.1), F = 0.2, f = 1]$.

This, together with Eq. (4.4), indicates that

$$W_I + W_{IF} = W_F + W_{FI}. \tag{5.3}$$

After transforming the integrations with respect to β into the infinite summations, Eqs. (4.7) and (4.10) can be also used for $y = 0^-$. Thus, the discontinuity of W at $y = 0$ is due to $W_{IE}(y = 0^+)$ in Eq. (4.8) and W_{FE} $(y = 0^-)$ in Eq. (4.16). Since $W_{IE} = W_{FE}$, as explained above Eq. (4.14). The discontinuity is due to the fact that W_{IE} or W_{FE} is discontinuous at $y = 0$.

When the semi-infinite ice sheet is absent, or the upper water surface is fully the free surface, the waves generated by the source are mainly dependent on the dispersion relation, $K_f(\alpha, \beta) = 0$. We may rewrite it as

$$\hat{k} \tanh\left(\hat{k}/F_H^2\right) - (\tau + \hat{\alpha})^2 = 0, \tag{5.4}$$

where

$$(\hat{\alpha}, \hat{k}, \tau, F_H) = (\alpha F^2, kF^2, fF, U/\sqrt{gH}). \tag{5.5}$$

Equation (5.4) indicates that the waves are dependent on both τ and F_H. For steady flows with $f = 0$, the transverse waves will disappear behind the source for supercritical speed $F_H > 1$, while for $f \neq 0$, there still exists time-harmonic transverse waves even for $F_H > 1$ [46]. When the source is moving near the edge of a semi-infinite ice sheet, the waves will be affected by both the free-surface boundary condition with $y \leqslant 0^-$ and ice-covered boundary condition with $y \geqslant 0^+$.

Figure 4 shows the free-surface wave elevation at $y = 0^-$ along the ice edge for a given Froude number $F = 0.2$ and wave radian frequency $f = 1$, with different ice-sheet thickness h. The source position is at $(\xi, \eta, \zeta) = (0, -0.5, -0.1)$. Figure 5 depicts the corresponding ice-sheet deflection at

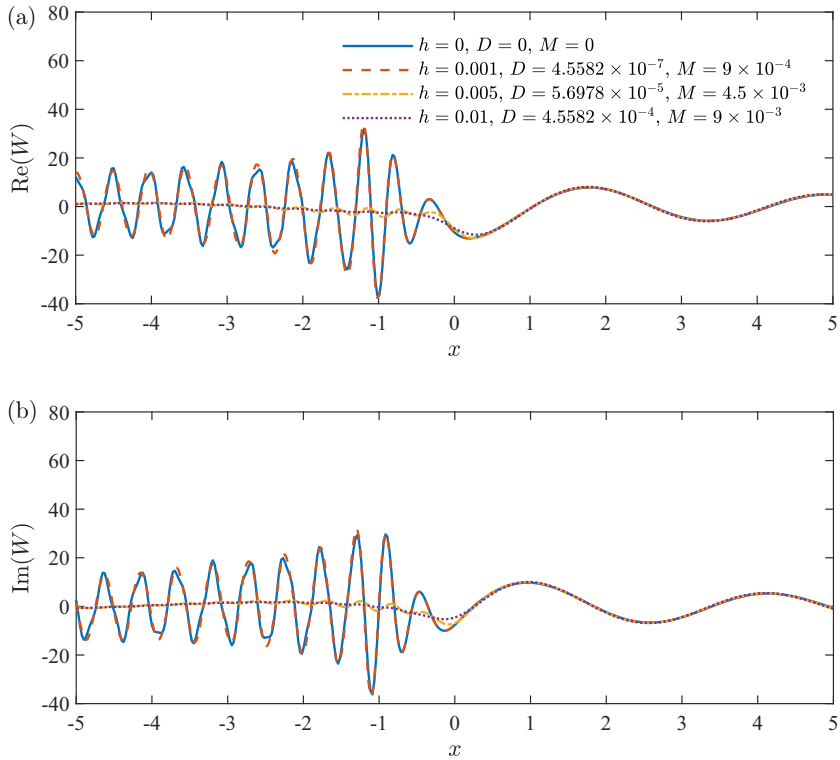

FIG. 5. The ice-sheet deflection W at $y = 0^+$, with different ice thickness h. (a) Real part of W; (b) imaginary part of W $[(\xi, \eta, \zeta) = (0, -0.5, -0.1), F = 0.2, f = 1]$.

$y = 0^+$ along the ice edge. It can be seen from Figs. 4 and 5 that the waves along $y = 0^+$ and $y = 0^-$ at $x > 0$ are much longer than those at $x < 0$. For longer waves, both W at $y = 0^+$ and $y = 0^-$ with different h are much closer to that with $h = 0$. This is because that at larger wavelength or smaller wave number, the dispersion relations for flexural-gravity wave and free-surface wave become closer. From Eq. (E17) for the far-field wave component of the Green function, we have that the wave motion is mainly determined by components with wave number obtained from the dispersion relation. Similar dispersion relation leads to similar wave elevations. As the wave becomes shorter or the wave number becomes larger at $x < 0$, the effect of ice-sheet thickness becomes obvious. When $h \to 0$, both W at $y = 0^+$ and $y = 0^-$ tend to W_F, as can be expected. As h increases, however, the free-surface wave elevations W at $y = 0^-$ for different h depart from each other. Similar results can be also observed for the ice-sheet deflection W at $y = 0^+$. Generally, the amplitude of both W at $y = 0^+$ and $y = 0^-$ decreases with the increase of h, i.e., the ice sheet will depress the free-surface wave elevation along the edge.

Figure 6 shows the free-surface wave elevation at $y = 0^-$ along the ice edge for a given Froude number $F = 0.2$ and ice-sheet thickness $h = 0.01$. Four wave radian frequencies are considered, i.e., $f = 1,\ 2,\ 3,\ 4$. The source position is taken to be the same as that in Fig. 4. The corresponding ice-sheet deflection at $y = 0^+$ along the ice edge is depicted in Fig. 7. In Figs. 8 and 9, W_F for infinite free surface and W_I for infinite ice sheet are provided, respectively. It can be observed from Figs. 6 and 7 that the amplitude of the wave at both $y = 0^-$ and $y = 0^+$ ahead of the source decreases with the increases of f. For infinite free surface, Fig. 8 shows that W_F ahead of the source is nearly zero when $f \geqslant 2$. This is very much related to the critical τ value, which is 1/4 [5] when H is infinite and is affected by water depth when H is finite (e.g., Ref. [47]), while for the water surface covered

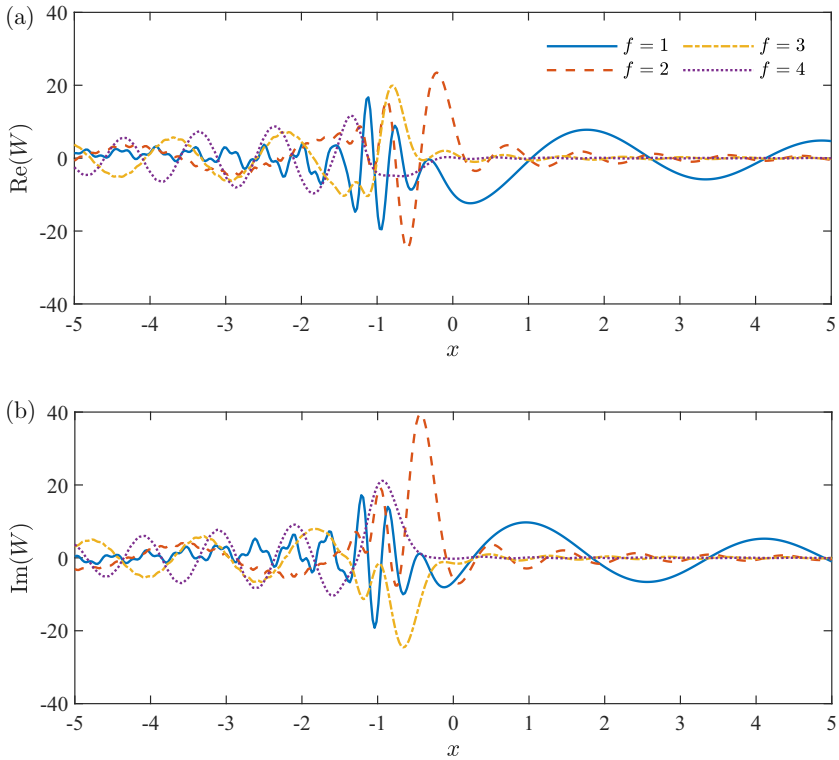

FIG. 6. The free-surface wave elevation W at $y = 0^-$, with different radian frequency f. (a) Real part of W; (b) imaginary part of W $[(\xi, \eta, \zeta) = (0, -0.5, -0.1), F = 0.2, h = 0.01, D = 4.5582\times10^{-4}, M = 9\times10^{-3}]$.

by an ice sheet of infinite extent, waves ahead of the source are visible at $1 \leqslant f \leqslant 4$, as shown in Fig. 9. When the water surface is covered by a semi-infinite ice sheet and the source is located in the free-surface part, ahead of the source, W is larger than W_F at $y = 0^-$ while W is smaller than W_I at $y = 0^+$ for $f \geqslant 2$. This is because the free-surface waves generated by the source will transmit into the ice-covered region, and propagate in form of flexural-gravity waves. The waves dominated by elasticity propagate ahead of the source, and the deflection of the ice sheet W at $y = 0^+$ will lead to the free-surface wave elevation W at $y = 0^-$. As only part of the free-surface wave energy can transmit into the ice-covered region, W at $y = 0^+$ is smaller than that of an infinite ice sheet.

C. The far-field free-surface and ice-sheet deflection wave patterns

The far-field features of the wave pattern can be further determined by applying the stationary phase method to Eq. (E17), with [48]

$$\psi = \alpha\bar{x} + \beta\bar{y} \tag{5.6}$$

as the phase function along the dispersion curves. The stationary points are defined by

$$\psi' = \alpha'\bar{x} + \beta'\bar{y} = 0, \tag{5.7}$$

where the prime denotes derivative with respect to S (see Appendix E). The wavelength corresponding to a stationary point of Eq. (5.7) is $\lambda = 2\pi/k$. Introducing the polar coordinate system, or $(\bar{x}, \bar{y}) = R(\cos\ \vartheta,\ \sin\ \vartheta)$, and noticing

$$\frac{dK}{dS} = K_\alpha\alpha' + K_\beta\beta' = 0 \tag{5.8}$$

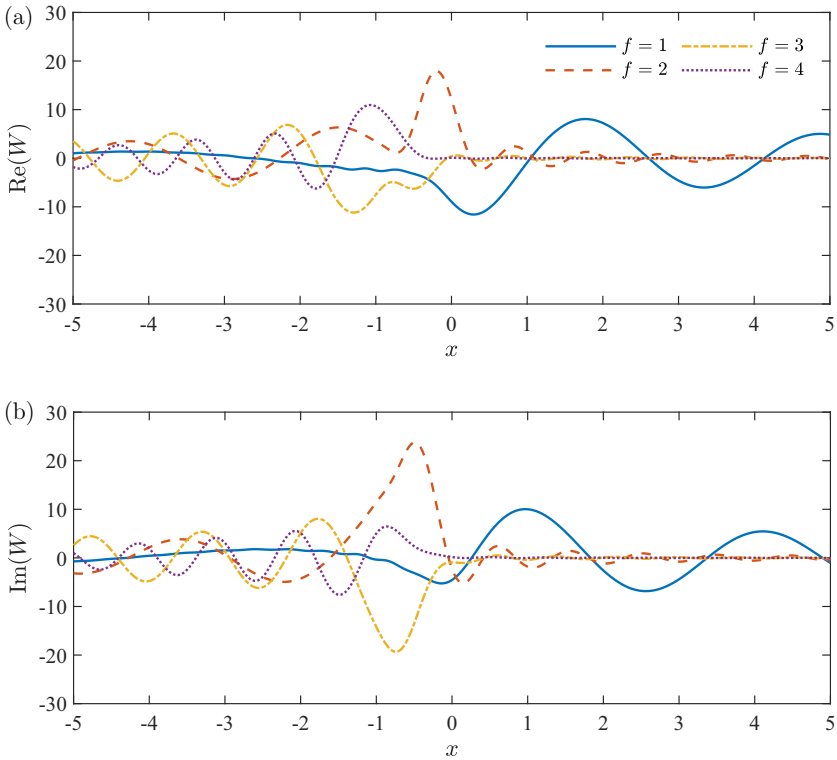

FIG. 7. The ice-sheet deflection W at $y = 0^+$, with different radian frequency f. (a) Real part of W; (b) imaginary part of W $[(\xi, \eta, \zeta) = (0, -0.5, -0.1),\ F = 0.2,\ h = 0.01,\ D = 4.5582 \times 10^{-4},\ M = 9 \times 10^{-3}]$.

along the dispersion curve $K(\alpha, \beta) = 0$, we can rewrite Eq. (5.7) as

$$\bar{x}K_\beta - \bar{y}K_\alpha = R|\nabla K| \sin(\gamma - \vartheta) = 0. \tag{5.9}$$

Here, γ is the angle between the unit normal vector to the dispersion curve and the α axis, i.e.,

$$(K_\alpha, K_\beta) = |\nabla K|(\cos\ \gamma,\ \sin\ \gamma). \tag{5.10}$$

Equation (5.9) indicates that at a stationary point on the dispersion curve, the direction of the wave is either $\gamma = \vartheta$ with $\mathrm{sgn}(\Psi) = 1$ or $\gamma = \vartheta + \pi$ with $\mathrm{sgn}(\Psi) = -1$. For flexural-gravity wave and free-surface wave, we have, respectively, $\Psi = \Psi_i$ and $\Psi = \Psi_f$, as given in Eqs. (3.27) and (3.31).

For a wave in the form of $\exp[-i(\psi - ft)]$, the phase velocity $\vec{v}_p$ and group velocity $\vec{v}_g$ can be given as [36]

$$\vec{v}_p = (\alpha, \beta)\frac{f}{k^2}, \tag{5.11}$$

and

$$\vec{v}_g = \left(\frac{\partial f}{\partial \alpha}, \frac{\partial f}{\partial \beta}\right) = -(K_\alpha, K_\beta)\frac{1}{K_{,f}}, \tag{5.12}$$

respectively, where $K_{,f} = \partial K/\partial f$ and $k = \sqrt{\alpha^2 + \beta^2}$. Invoking Eqs. (5.6) and (5.9), the curves along which the phase ψ is constant are given as

$$(\bar{x}_m, \bar{y}_m) = \psi_m^{\pm}(K_\alpha, K_\beta)/(\alpha K_\alpha + \beta K_\beta), \tag{5.13}$$

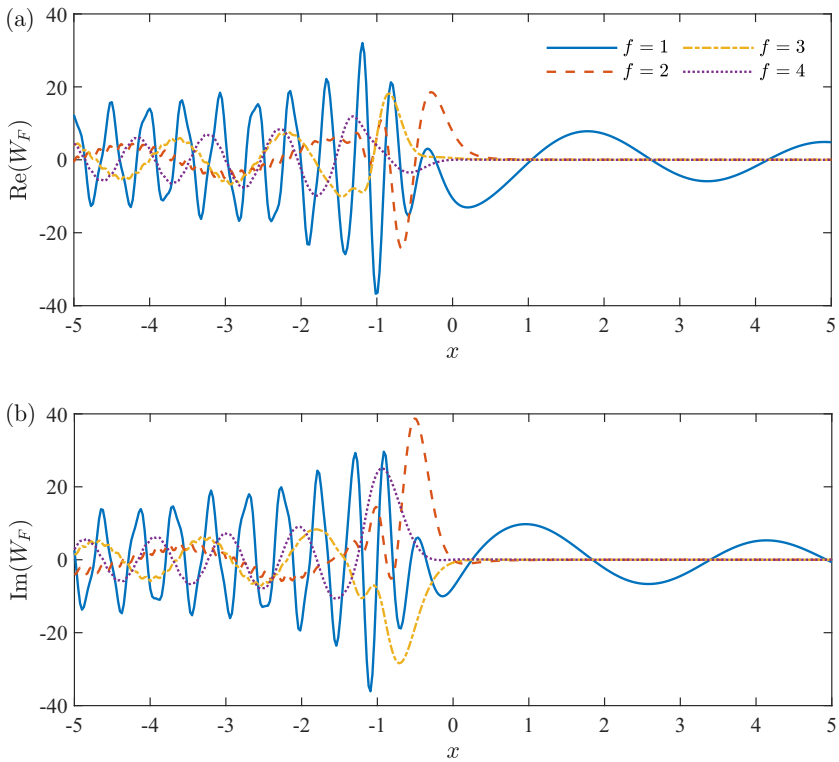

FIG. 8. The free-surface wave elevation W_F at $y = 0^-$, with different radian frequency f. (a) Real part of W_F; (b) imaginary part of W_F $[(\xi, \eta, \zeta) = (0, -0.5, -0.1)$, $F = 0.2$, $h = 0.01$, $D = 4.5582 \times 10^{-4}$, $M = 9 \times 10^{-3}]$.

where

$$\psi_m^{\pm} = \psi_0 \pm 2m\pi \ (m = 1, 2, \ldots), \tag{5.14}$$

and ψ_0 is the solution of Eq. (5.7). Here, the phase jump at the cusp line is ignored, where the cusp angle can be determined by requiring the second-order derivative of the phase function equal to zero or $\psi'' = 0$ [36]. From (E17), we have

$$\mathrm{sgn}[(\bar{x}K_\alpha + \bar{y}K_\beta)\Psi] > 0. \tag{5.15}$$

In Eq. (5.14), only those m which satisfy Eq. (5.15) can be taken. From Eqs. (5.12) and (5.15), we have

$$(\bar{x}_m, \bar{y}_m) \cdot \vec{v}_g = -\frac{\bar{x}_m K_\alpha + \bar{y}_m K_\beta}{K_{,f}} > 0, \tag{5.16}$$

where $\Psi = -K_{,f}$ has been used. This indicates that the wave energy is propagating away from the source, which is consistent with the radiation condition.

We may consider the wave pattern when the field point p is sufficiently far from the source point q, or $R = \sqrt{\bar{x}^2 + \bar{y}^2} \to \infty$ with $(\bar{x}, \bar{y}) = (x-\xi, y-\eta)$. Invoking Eq. (E17) in Appendix E, Eqs. (4.3) to (4.6) can be approximated as

$$\lim_{R\to\infty} W \approx -\sum_{m=1}^{M_I} \int_{S_m^I} \Lambda_i(\alpha, \beta) w_i(\alpha, \beta) \frac{e^{-i(\alpha\bar{x}+\beta\bar{y})}}{|\nabla K_i|} dS, \tag{5.17}$$

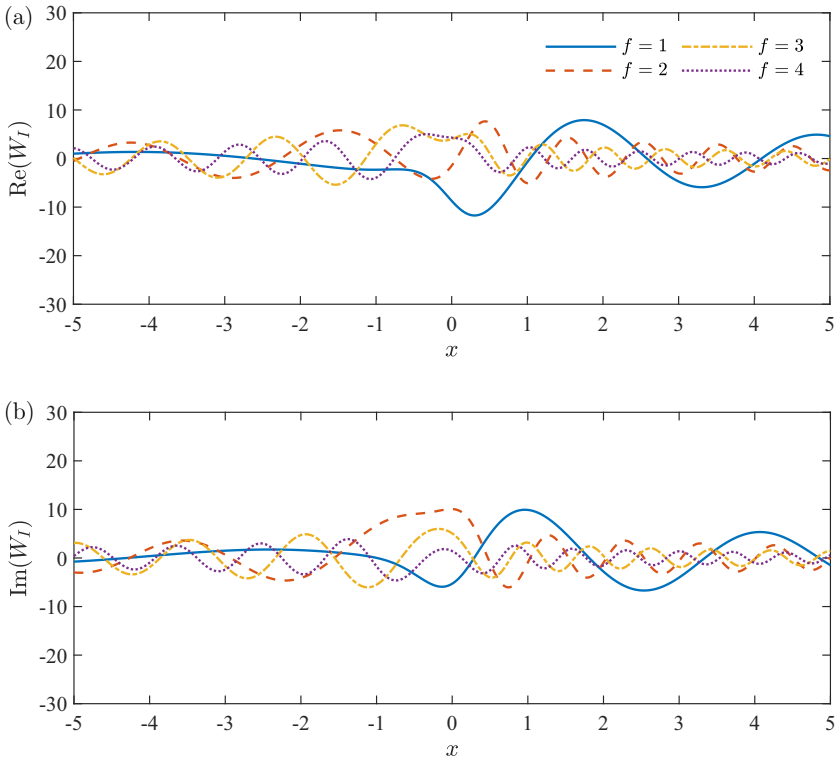

FIG. 9. The ice-sheet deflection W_I at $y = 0^+$, with different radian frequency f. (a) Real part of W_I; (b) imaginary part of W_I $[(\xi, \eta, \zeta) = (0, -0.5, -0.1),\ F = 0.2,\ h = 0.01,\ D = 4.5582 \times 10^{-4},\ M = 9 \times 10^{-3}]$.

where

$$w_i(\alpha, \beta) = w_I(\alpha, \beta) + w_{IF}(\alpha, \beta) + w_{IE}(\alpha, \beta), \tag{5.18}$$

$$w_I(\alpha, \beta) = (f + \alpha F)\hat{C}(\zeta), \tag{5.19}$$

$$w_{IF}(\alpha, \beta) = \frac{M_-(\alpha, \beta)K_-(\alpha, \beta)}{f + \alpha F} k \tanh(kH) e^{-i\beta\eta}, \tag{5.20}$$

$$w_{IE}(\alpha, \beta) = \frac{[a(\alpha) + b(\alpha)\beta]K_-(\alpha, \beta)}{f + \alpha F} k \tanh(kH) e^{-i\beta\eta}, \tag{5.21}$$

$$\Lambda_i(\alpha, \beta) = \mathrm{sgn}[\bar{x}K_{i,\alpha}(\alpha, \beta) + \bar{y}K_{i,\beta}(\alpha, \beta)] + \mathrm{sgn}[\Psi_i(\alpha, \beta)]. \tag{5.22}$$

S_m^I $(m = 1, \ldots, M_I)$ in Eq. (5.17) represents the mth segment of the dispersion curve in the (α, β) plane with $K_i(\alpha, \beta) = 0$. Similarly, Eqs. (4.11) to (4.14) can be approximated as

$$\lim_{R\to\infty} W \approx -\sum_{m=1}^{M_F} \int_{S_m^F} \Lambda_f(\alpha, \beta) w_f(\alpha, \beta) \frac{e^{-i(\alpha\bar{x}+\beta\bar{y})}}{|\nabla K_f|} dS, \tag{5.23}$$

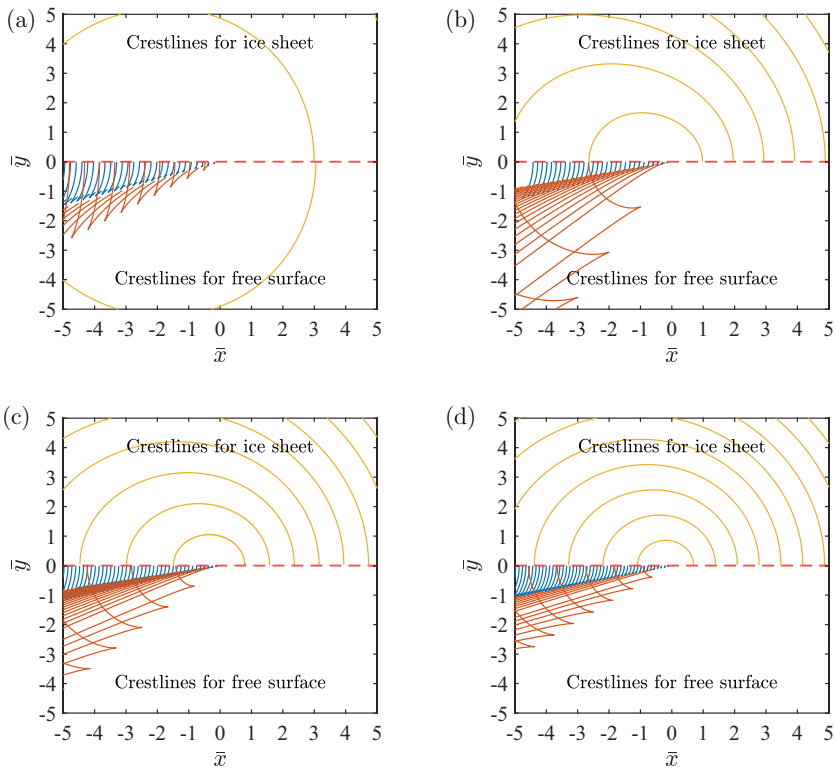

FIG. 10. Crestlines of the free-surface wave at $\bar{y} \leqslant 0^-$ and flexural-gravity wave at $\bar{y} \geqslant 0^+$, with different radian frequency f. (a) is for $f = 1$; (b) is for $f = 2$; (c) is for $f = 3$; and (d) is for $f = 4$ $[(\xi, \eta, \zeta) = (0, -0.5, -0.1), F = 0.2, h = 0.01, D = 4.5582 \times 10^{-4}, M = 9 \times 10^{-3}]$.

where

$$w_f(\alpha, \beta) = w_F(\alpha, \beta) + w_{FI}(\alpha, \beta) + w_{FE}(\alpha, \beta), \tag{5.24}$$

$$w_F(\alpha, \beta) = (f + \alpha F)\hat{C}(\zeta), \tag{5.25}$$

$$w_{FI}(\alpha, \beta) = -\frac{M_+(\alpha, \beta)}{(f + \alpha F)K_+(\alpha, \beta)} k \tanh(kH) e^{-i\beta\eta}, \tag{5.26}$$

$$w_{FE}(\alpha, \beta) = \frac{a(\alpha) + b(\alpha)\beta}{(f + \alpha F)K_+(\alpha, \beta)} k \tanh(kH) e^{-i\beta\eta}, \tag{5.27}$$

$$\Lambda_f(\alpha, \beta) = \mathrm{sgn}[\bar{x}K_{f,\alpha}(\alpha, \beta) + \bar{y}K_{f,\beta}(\alpha, \beta)] + \mathrm{sgn}[\Psi_f(\alpha, \beta)], \tag{5.28}$$

and S_m^F $(m = 1, \ldots, M_F)$ represents the mth segment of the dispersion curve in the (α, β) plane with $K_f(\alpha, \beta) = 0$.

Figure 10 shows the crestlines for fully free-surface wave W_F at $\bar{y} \leqslant 0^-$ and fully flexural-gravity wave W_I at $\bar{y} \geqslant 0^+$. The Froude number is taken to be $F = 0.2$. Four wave radian frequencies are considered, i.e., $f = 1, 2, 3, 4$. For flexural-gravity wave dominated by the dispersion equation $K_i(\alpha, \beta) = 0$, the wave system is composed of ring waves, and within the computed range of wave radian frequency the wavelength decreases with the increase of f. For free-surface wave dominated by the dispersion equation $K_f(\alpha, \beta) = 0$, at a smaller wave radian frequency ($f = 1$), the wave system is composed of inner-V waves, outer-V waves, and the ring waves. As the wave radian frequency increases, the ring waves disappear when τ is larger than a critical value, and the outer-V

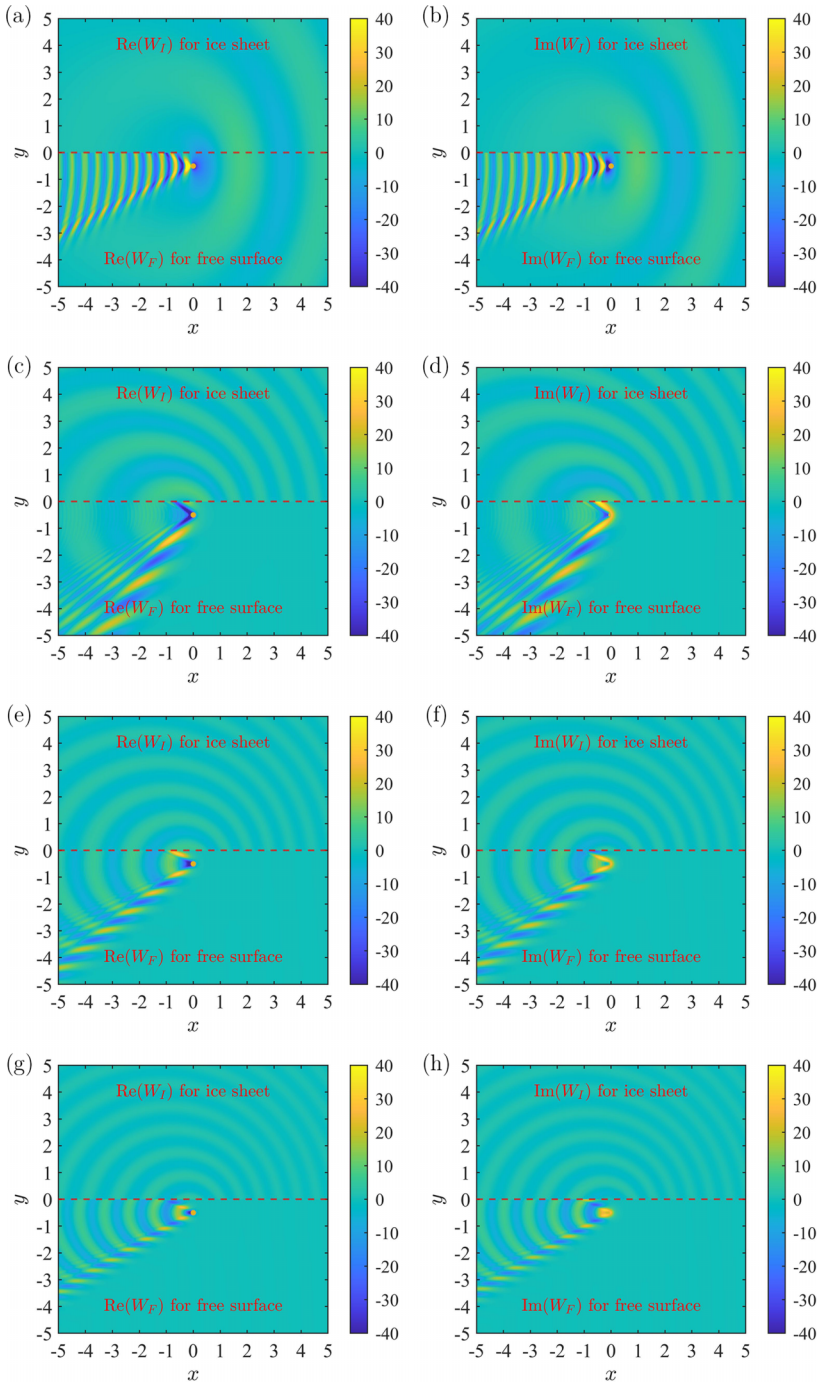

FIG. 11. The free-surface wave elevation W_F at $y \leqslant 0^-$ and ice-sheet deflection W_I at $y \geqslant 0^+$, with different radian frequency f. (a), (b) are for $f = 1$; (c), (d) are for $f = 2$; (e), (f) are for $f = 3$; and (g), (h) are for $f = 4$ $[(\xi, \eta, \zeta) = (0, -0.5, -0.1), F = 0.2, h = 0.01, D = 4.5582 \times 10^{-4}, M = 9 \times 10^{-3}]$.

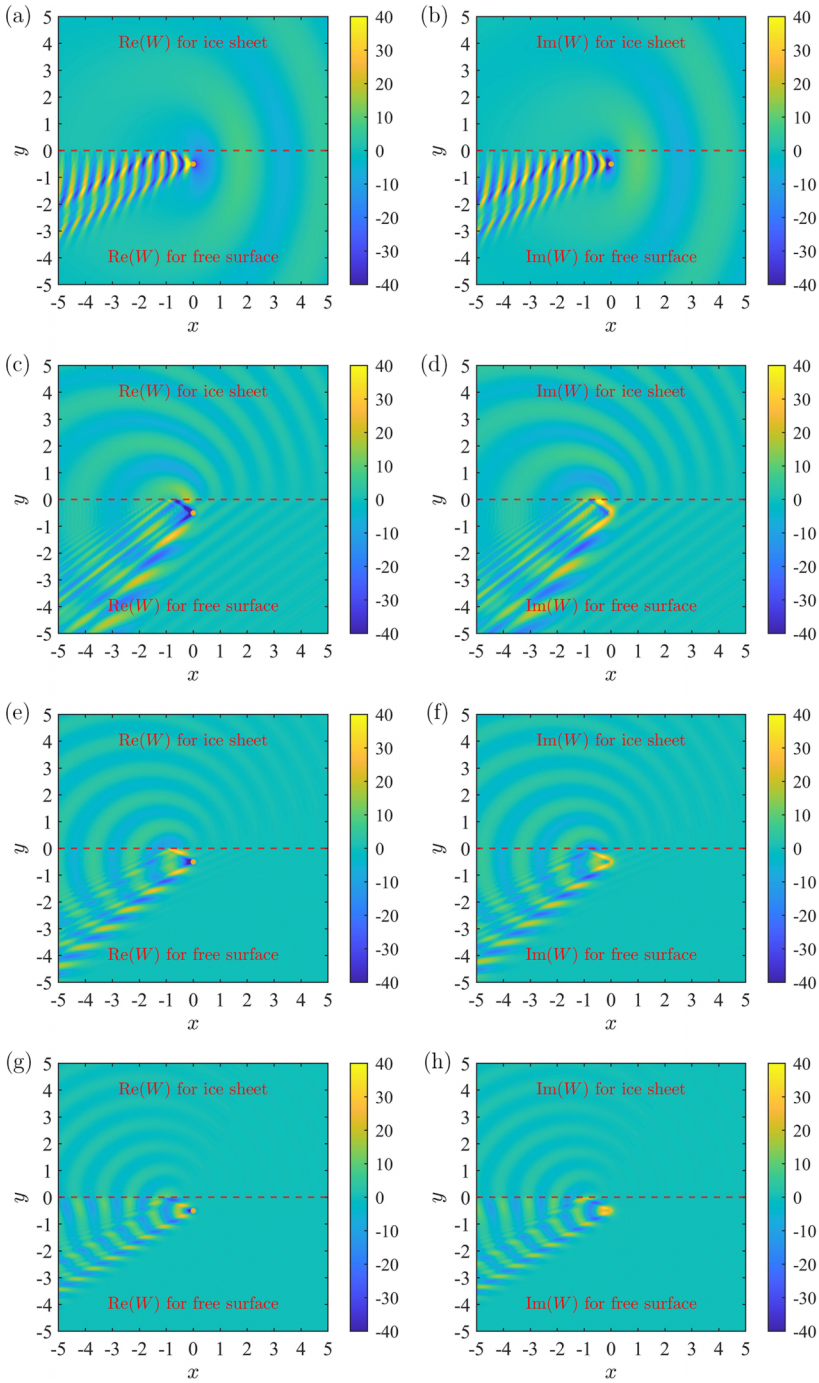

FIG. 12. The free-surface wave elevation W at $y \leqslant 0^-$ and ice-sheet deflection W at $y \geqslant 0^+$, with different radian frequency f. (a), (b) are for $f = 1$; (c), (d) are for $f = 2$; (e), (f) are for $f = 3$; and (g), (h) are for $f = 4$ $[(\xi, \eta, \zeta) = (0, -0.5, -0.1), F = 0.2, h = 0.01, D = 4.5582 \times 10^{-4}, M = 9 \times 10^{-3}]$.

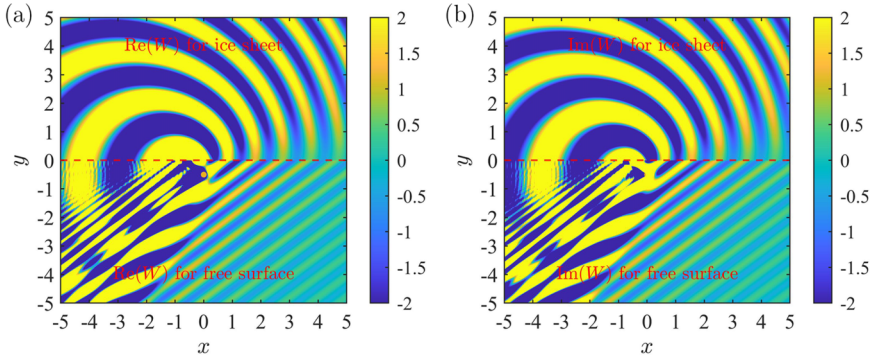

FIG. 13. The free-surface wave elevation W at $y \leqslant 0^-$ and ice-sheet deflection W at $y \geqslant 0^+$. (a), (b) are the same as (c), (d) in Fig. 12 but with a higher color resolution $[(\xi, \eta, \zeta) = (0, -0.5, -0.1), F = 0.2, h = 0.01, D = 4.5582 \times 10^{-4}, M = 9 \times 10^{-3}]$.

waves become the partial ring and fan waves. For the ring waves, the wavelengths for free-surface wave and flexural-gravity wave are close to each other. This can be more clearly observed from Fig. 11, which shows the contour plot of free-surface wave elevation W_F in Eq. (4.15) at $y \leqslant 0^-$ and ice-sheet deflection W_I in Eq. (4.7) at $y \geqslant 0^+$. The source position is taken to be at $(\xi, \eta, \zeta) = (0, -0.5, -0.1)$. It can be also observed from Fig. 11 that the amplitude of the inner-V waves is generally smaller than that of the ring waves or partial ring and fan waves.

Figure 12 depicts the contour plot of wave patterns when the upper water surface is covered by an ice sheet of semi-infinite extent, i.e., the free-surface wave elevation in Eq. (4.11) at $y \leqslant 0^-$ and ice-sheet deflection in Eq. (4.3) at $y \geqslant 0^+$. It can be observed from Fig. 12 that the free-surface wave pattern at $y \leqslant 0^-$ will be very much affected by the semi-infinite ice sheet at $y \geqslant 0^+$. Due to the change of the physical properties of upper water surface, the wave energy generated by the source will be partially reflected back to the region $y \leqslant 0^-$. Compared with Fig. 11, there are two systems of free-surface wave in Fig. 12. The outer-V wave is very much similar to W_F itself. Then, W_F will propagate towards the ice sheet. It will be reflected back to the free surface by the ice sheet and its edge. The reflection forms an inner-V wave. When $f = 1$, the ring waves appear ahead of the source both in the ice-sheet domain and the free-surface domain. When $f = 2$ in Figs. 12(c) and 12(d), the wave ahead of the source in the free-surface domain is no longer visible, as in Figs. 12(e) to 12(h) for $f = 3,\ 4$. Figures 12(c) and 12(d) are produced in Figs. 13(a) and 13(b) with a higher color resolution or smaller scale. It is interesting to see that even though the far-field wave may not appear ahead of the source on the free-surface side, the local waves are still visible, which is different from the free-surface-only problem. This may be very much due to the fact the waves ahead of the source on the ice sheet side have transmitted into the free surface.

VI. CONCLUSIONS

The problem of wave motion due to a point source pulsating and advancing at constant forward speed along a semi-infinite ice sheet in finite water depth has been solved. The mathematical model is based on the linear velocity potential theory for fluid flow and thin elastic plate model for ice sheet. Then, the Green function, which satisfies all the boundary conditions, is derived through the Fourier transform and Wiener-Hopf technique. The solution shows that when the upper surface is composed of two parts of semi-infinite extent, the wave motion below each surface can be decomposed into three parts. One is due to the upper surface itself, either free surface or the ice sheet, and the other two are due to interactions with the other upper surface and with the intersection line of these two surfaces, i.e., the ice edge.

For wave motions along the ice edge, the wavelength of the waves ahead of the source is much longer than that of the waves behind the source. Thus, the wave elevation ahead of the source for different ice thickness all tend to that for fully free surface, while behind the source, the ice thickness has a very stronger effect on the wave elevation. The amplitude of the wave on both sides of the ice edge decreases with the increase of ice thickness, which indicates that the ice sheet will depress the free-surface wave elevation along the edge.

When the source is below the free surface, the free-surface wave pattern has two V-shaped components. The outer-V wave is very similar to the common free-surface wave without the ice sheet, while the inner-V wave is mainly due to the reflection of the outer-V wave by the ice sheet and ice edge. When τ is larger than a critical value, the free-surface ring wave far ahead of the source may disappear. However, the ice-sheet deflection ring wave is still quite visible ahead of the source, which may affect the local free-surface wave ahead of the source.

ACKNOWLEDGMENT

This work is supported by the National Natural Science Foundation of China (Grants No. 52071162, No. 12372242, and No. 52101315).

APPENDIX A: THE REAL ROOT OF THE DISPERSION EQUATION

We assume κ_0 as the positive real root of the dispersion equation $\mathcal{K}_i(\kappa_0, f) = 0$ at a given f. The replacement of the real frequency f with a complex frequency $\hat{f} = f - i\varepsilon$ ($\varepsilon \to 0^+$) will change the real root κ_0 to a complex root $\hat{\kappa}_0$ in the complex plane, or $\mathcal{K}_i^\varepsilon(\hat{\kappa}_0, \hat{f}) = 0$. Here, $\mathcal{K}_i^\varepsilon(k, \hat{f}) \equiv K_i^\varepsilon(\alpha, \beta)$ in Eq. (3.25), or

$$\mathcal{K}_i^\varepsilon(k, \hat{f}) \approx \mathcal{K}_i(k, f) + i\varepsilon\mathcal{P}_i(k, f), \tag{A1}$$

where

$$\mathcal{K}_i(k, f) = [Dk^4 - M(f + \alpha F)^2 + 1]k\tanh(kH) - (f + \alpha F)^2, \tag{A2}$$

$$\mathcal{P}_i(k, f) = 2(f + \alpha F)[Mk\tanh(kH) + 1]. \tag{A3}$$

The Taylor expansion of $\mathcal{K}_i^\varepsilon$ at $k = \kappa_0$ and $\varepsilon = 0$ provides

$$\mathcal{K}_i^\varepsilon(k, \hat{f}) \approx (\kappa - \kappa_0)\mathcal{K}_i'(\kappa_0, f) + i\varepsilon\mathcal{P}_i(\kappa_0, f), \tag{A4}$$

where

$$\begin{aligned}\mathcal{K}_i'(k, f) &= \frac{\partial\mathcal{K}_i(k, f)}{\partial k}\\ &= [Dk^4 - M(f + \alpha F)^2 + 1][\tanh(kH) + kH\,\mathrm{sech}^2(kH)] + 4Dk^4\tanh(kH).\end{aligned} \tag{A5}$$

From Eq. (A4), we have

$$\hat{\kappa}_0 = \kappa_0 - i\varepsilon\Gamma(\kappa_0, f), \tag{A6}$$

where

$$\Gamma(\kappa_0, f) = \frac{\mathcal{P}_i(\kappa_0, f)}{\mathcal{K}_i'(\kappa_0, f)}. \tag{A7}$$

Invoking Eqs. (A2) and (A3), we have

$$\Gamma(\kappa_0, f) = \frac{1}{f + \alpha F}\frac{\left(D\kappa_0^4 + 1\right)\kappa_0\tanh(\kappa_0 H)}{2D\kappa_0^4\tanh(\kappa_0 H) + \frac{(f+\alpha F)^2}{2\kappa_0} + \frac{H(f+\alpha F)^2}{\sinh(2\kappa_0 H)}}. \tag{A8}$$

As $\varepsilon \to 0^+$, the only effect of $\Gamma(\kappa_0, f)$ on Eq. (A6) is the sign of the imaginary part. In Eq. (A8), only the term $f + \alpha F$ may change its sign, and the rest is always positive. Thus, we may rewrite

Eq. (A6) as

$$\hat{\kappa}_0 = \kappa_0 - i\varepsilon_1 \mathrm{sgn}(f + \alpha F) = \kappa_0 - i\varepsilon_1 \mathrm{sgn}(f/\kappa_0 + F\cos\theta), \tag{A9}$$

where sgn is the sign function, $\varepsilon_1 \to 0^+$ as $\varepsilon \to 0^+$, and Eq. (3.10) or $\alpha = \kappa_0 \cos\theta$ has been used.

APPENDIX B: THE FACTORIZATION OF EQ. (3.41)

From the Weierstrass factorization theorem, and noticing $K_i^\varepsilon(\alpha, 0) \neq 0$, we have

$$\tilde{K}_i^\varepsilon(\alpha, \beta) \equiv \cosh(kH) K_i^\varepsilon(\alpha, \beta) = e^{g(\beta)} \prod_{m=-2}^{\infty} \left(1 - \frac{\beta^2}{\chi_m^2}\right), \tag{B1}$$

which is convergent since $\chi_m \to im\pi$ as $m \to \infty$. This gives

$$\log\left[\tilde{K}_i^\varepsilon(\alpha, \beta)\right] = g(\beta) + \sum_{m=-2}^{\infty} \log\left(1 - \frac{\beta^2}{\chi_m^2}\right). \tag{B2}$$

Taking partial derivative with respect to β on both sides of Eq. (B2), we have

$$\frac{\tilde{K}_i^{\varepsilon\prime}(\alpha, \beta)}{\tilde{K}_i^\varepsilon(\alpha, \beta)} = g'(\beta) + \sum_{m=-2}^{\infty} \frac{2\beta}{\beta^2 - \chi_m^2}, \tag{B3}$$

where $\tilde{K}_i^{\varepsilon\prime}(\alpha, \beta) = \partial \tilde{K}_i^\varepsilon(\alpha, \beta)/\partial\beta$. We may apply the Mittag-Leffler theorem to the left-hand side of Eq. (B3), which provides

$$\frac{\tilde{K}_i^{\varepsilon\prime}(\alpha, \beta)}{\tilde{K}_i^\varepsilon(\alpha, \beta)} = g_1(\beta) + \sum_{m=-2}^{\infty} \left(\frac{1}{\beta - \chi_m} + \frac{1}{\beta + \chi_m}\right), \tag{B4}$$

where $\mathrm{Res}[\tilde{K}_i^{\varepsilon\prime}(\alpha, \pm\chi_m)/\tilde{K}_i^\varepsilon(\alpha, \pm\chi_m)] = 1$ has been used. Here, the summation in Eq. (B4) is convergent. As the first term on the right-hand side is analytical and obviously finite in the β plane, it must be independent of β based on Liouville's theorem. Let $\beta = 0$ in Eq. (B4). Since $\tilde{K}_i^{\varepsilon\prime}(\alpha, 0)/\tilde{K}_i^\varepsilon(\alpha, 0) = 0$ and the summation is zero, we obtain $g_1(\beta) = 0$. Invoking Eqs. (B3) and (B4), we have

$$g'(\beta) = 0. \tag{B5}$$

This means that $g(\beta)$ or $\exp[g(\beta)]$ is a constant at a given α, or $g(\beta)$ is a function of α only. Equation (3.26) provides

$$\lim_{\beta \to i\alpha} \tilde{K}_i^\varepsilon(\alpha, \beta) = -(f - i\varepsilon + \alpha F)^2, \tag{B6}$$

as $k = 0$. Together with Eqs. (3.37) and (B1), this gives

$$e^{g(\beta)} = -(f - i\varepsilon + \alpha F)^2 \prod_{m=-2}^{\infty} \frac{\chi_m^2}{\kappa_m^2}. \tag{B7}$$

Substituting Eq. (B7) into (B1), we have

$$\tilde{K}_i^\varepsilon(\alpha, \beta) = (f - i\varepsilon + \alpha F)^2 \prod_{m=-2}^{\infty} \frac{(\beta - \chi_m)(\beta + \chi_m)}{\kappa_m^2}. \tag{B8}$$

Following a similar procedure, we can obtain

$$\tilde{K}_f^\varepsilon(\alpha, \beta) \equiv \cosh(kH) K_f^\varepsilon(\alpha, \beta) = (f - i\varepsilon + \alpha F)^2 \prod_{m=0}^{\infty} \frac{(\beta - \gamma_m)(\beta + \gamma_m)}{k_m^2}. \tag{B9}$$

Based on the definition of $K_\pm$ in Eq. (3.41), and using (B8) and (B9), we can write

$$K_\pm(\alpha,\beta) = \frac{(\beta \pm \chi_{-2})(\beta \pm \chi_{-1})}{\kappa_{-2}\kappa_{-1}} \prod_{m=0}^{\infty} \frac{k_m(\beta \pm \chi_m)}{\kappa_m(\beta \pm \gamma_m)}, \tag{B10}$$

where $K_i^\varepsilon(\alpha,\beta)/K_f^\varepsilon(\alpha,\beta) = \tilde{K}_i^\varepsilon(\alpha,\beta)/\tilde{K}_f^\varepsilon(\alpha,\beta)$ has been used.

APPENDIX C: THE COMPUTATION OF MATRIX EQUATION (3.64)

We may first assume that the source is located in the free-surface part, i.e., $\eta \leqslant 0^-$. Since $y \to 0^+$ in Eq. (3.64), we have $y-\eta > 0$. Then, using the Cauchy residual theorem in the lower half plane of β and noticing that singularities are due to the roots of $K_i(\alpha,\beta) = 0$ at $\beta = -\chi_m$, we can rewrite Eqs. (3.57) and (3.58) as

$$\widehat{I}_1(\alpha,y) = -2\pi i \sum_{m=-2}^{\infty} e^{i\chi_m y}\kappa_m \tanh(\kappa_m H)\frac{K_-(\alpha,-\chi_m)}{K'_i(\alpha,-\chi_m)}, \tag{C1}$$

$$\widehat{I}_2(\alpha,y) = 2\pi i \sum_{m=-2}^{\infty} e^{i\chi_m y}\chi_m\kappa_m \tanh(\kappa_m H)\frac{K_-(\alpha,-\chi_m)}{K'_i(\alpha,-\chi_m)}. \tag{C2}$$

For the integral (3.59), by using Eq. (3.46) we can rewrite it as

$$\begin{aligned}\widehat{I}_3(\alpha,y) = &\int_{-\infty}^{+\infty} e^{-i\beta(y-\eta)}\hat{C}(k,\zeta)\left[\frac{k\tanh(kH)J(\alpha,\beta)}{K_i^\varepsilon(\alpha,\beta)K_f^\varepsilon(\alpha,\beta)} + \frac{(f-i\varepsilon+\alpha F)^2}{K_i^\varepsilon(\alpha,\beta)}\right]d\beta \\ &- \int_{-\infty}^{+\infty} e^{-i\beta y}\left[k\tanh(kH)\frac{K_-(\alpha,\beta)}{K_i^\varepsilon(\alpha,\beta)}\sum_{m=0}^{\infty}\frac{e^{-i\gamma_m\eta}\hat{C}(k_m,\zeta)J(\alpha,-\gamma_m)}{K_-(\alpha,-\gamma_m)K_f^{\varepsilon\prime}(\alpha,-\gamma_m)(\beta+\gamma_m)}\right]d\beta,\end{aligned} \tag{C3}$$

which can be further converted to a series as

$$\widehat{I}_3(\alpha,y) = 2\pi i \sum_{m=-2}^{\infty}\frac{e^{i\chi_m y}\kappa_m\tanh(\kappa_m H)K_-(\alpha,-\chi_m)}{K'_i(\alpha,-\chi_m)}\sum_{j=0}^{\infty}\frac{e^{-i\gamma_j\eta}\hat{C}(k_j,\zeta)J(\alpha,-\gamma_j)}{K_-(\alpha,-\gamma_j)K'_f(\alpha,-\gamma_j)(\gamma_j-\chi_m)}. \tag{C4}$$

In Eq. (C4), the following relation has been used:

$$\frac{J(\alpha,-\chi_m)}{K_f(\alpha,-\chi_m)} = -\frac{(f+\alpha F)^2}{\kappa_m\tanh(\kappa_m H)}. \tag{C5}$$

The elements of the matrix equation (3.64) involve the partial derivative of $\widehat{I}_1(\alpha,y)$, $\widehat{I}_2(\alpha,y)$, and $\widehat{I}_3(\alpha,y)$ with respect to y up to the third order at $y=0$, or

$$\widehat{I}_1^{(n)}(\alpha,0) = -2\pi i^{n+1}\sum_{m=-2}^{\infty}\chi_m^n\kappa_m\tanh(\kappa_m H)\frac{K_-(\alpha,-\chi_m)}{K'_i(\alpha,-\chi_m)}, \tag{C6}$$

$$\widehat{I}_2^{(n)}(\alpha,0) = 2\pi i^{n+1}\sum_{m=-2}^{\infty}\chi_m^{n+1}\kappa_m\tanh(\kappa_m H)\frac{K_-(\alpha,-\chi_m)}{K'_i(\alpha,-\chi_m)}, \tag{C7}$$

$$\widehat{I}_3^{(n)}(\alpha,0) = 2\pi i^{n+1}\sum_{m=-2}^{\infty}\frac{\chi_m^n\kappa_m\tanh(\kappa_m H)K_-(\alpha,-\chi_m)}{K'_i(\alpha,-\chi_m)}\sum_{j=0}^{\infty}\frac{e^{-i\gamma_j\eta}\hat{C}(k_j,\zeta)J(\alpha,-\gamma_j)}{K_-(\alpha,-\gamma_j)K'_f(\alpha,-\gamma_j)(\gamma_j-\chi_m)}, \tag{C8}$$

where $n = 1, 2, 3$. Because κ_m is the root of the dispersion equation (3.26), we have

$$\kappa_m \tanh(\kappa_m H) = \frac{(f + \alpha F)^4}{J(\alpha, -\chi_m) + (f + \alpha F)^2}, \tag{C9}$$

where Eq. (3.36) has been used. Substituting Eq. (C9) into Eqs. (C6) to (C8), it can be shown that the summations with respect to m are convergent.

APPENDIX D: THE GREEN FUNCTION FOR INFINITE ICE SHEET OR FREE SURFACE

When the water surface is covered by an ice sheet of infinite extent, we denote G_I as the Green function. $\widehat{G}_I$ and $\tilde{G}_I$ correspond to the Fourier transforms in (3.6) and (3.7), respectively. Similar to Eq. (3.11), we may write $\tilde{G}_I$ as

$$\tilde{G}_I = A_I(\alpha, \beta)C(k, z) - \frac{2}{k} e^{i\alpha\xi} e^{i\beta\eta} C(k, z_<) S(k, z_>). \tag{D1}$$

The left-hand side of Eq. (3.24) becomes zero, which provides

$$\begin{aligned} A_I(\alpha, \beta) = {} & \frac{2}{k} e^{i\alpha\xi} e^{i\beta\eta} \hat{C}(k, \zeta) \\ & \times \frac{[Dk^4 - M(f - i\varepsilon + \alpha F)^2 + 1]kC(k, 0) - (f - i\varepsilon + \alpha F)^2 S(k, 0)}{K_i^\varepsilon(\alpha, \beta)}. \end{aligned} \tag{D2}$$

Substituting Eq. (D2) into (D1), we have

$$\begin{aligned} \tilde{G}_I = {} & 2e^{i\alpha\xi} e^{i\beta\eta} \Bigg[\frac{C(k, \zeta)C(k, z)\tanh(kH) - C(k, z_<)S(k, z_>)}{k} \\ & + \hat{C}(k, \zeta)\hat{C}(k, z) \frac{Dk^4 - M(f - i\varepsilon + \alpha F)^2 + 1}{K_i^\varepsilon(\alpha, \beta)} \Bigg], \end{aligned} \tag{D3}$$

or

$$\begin{aligned} \tilde{G}_I = {} & e^{i\alpha\xi} e^{i\beta\eta} \Bigg[\frac{e^{-k|\zeta - z|} + e^{-k(\zeta + z + 2H)} - 2\mathcal{N}(\zeta, z)}{k} \\ & + 2\hat{C}(k, \zeta)\hat{C}(k, z) \frac{Dk^4 - M(f - i\varepsilon + \alpha F)^2 + 1}{K_i^\varepsilon(\alpha, \beta)} \Bigg], \end{aligned} \tag{D4}$$

where

$$C(k, \zeta)C(k, z)\tanh(kH) - C(k, z_<)S(k, z_>) = \frac{e^{-k|\zeta - z|} + e^{-k(\zeta + z + 2H)} - 2\mathcal{N}(\zeta, z)}{2}, \tag{D5}$$

has been used, with

$$\mathcal{N}(\zeta, z) = \frac{e^{-2kH}\{\cosh[k(\zeta + z + 2H)] + \cosh[k(\zeta - z)]\}}{1 + e^{-2kH}}. \tag{D6}$$

Taking inverse Fourier transform of $\tilde{G}_I$ with respect to β, we have

$$\begin{aligned} \widehat{G}_I = {} & \frac{1}{\sqrt{2\pi}} \int_{-\infty}^{+\infty} e^{i\alpha\xi} e^{i\beta(\eta - y)} \frac{e^{-k|\zeta - z|} + e^{-k(\zeta + z + 2H)} - 2\mathcal{N}(\zeta, z)}{k} d\beta \\ & + \frac{2}{\sqrt{2\pi}} \int_{-\infty}^{+\infty} e^{i\alpha\xi} e^{i\beta(\eta - y)} \hat{C}(k, \zeta)\hat{C}(k, z) \frac{Dk^4 - M(f - i\varepsilon + \alpha F)^2 + 1}{K_i^\varepsilon(\alpha, \beta)} d\beta. \end{aligned} \tag{D7}$$

Taking inverse Fourier transform of $\widehat{G}_I$ with respect to α, we have

$$G_I = G_0 + \frac{1}{\pi}\int_{-\infty}^{+\infty}\int_{-\infty}^{+\infty} e^{i\alpha(\xi-x)}e^{i\beta(\eta-y)} \times\left[\hat{C}(k,\zeta)\hat{C}(k,z)\frac{Dk^4 - M(f-i\varepsilon+\alpha F)^2+1}{K_i^{\varepsilon}(\alpha,\beta)} - \frac{\mathcal{N}(\zeta,z)}{k}\right]d\alpha d\beta, \tag{D8}$$

where

$$G_0 = \frac{1}{r_1} + \frac{1}{r_2}. \tag{D9}$$

Here, r_1 is the distance between p and q, and r_2 is the distance between p and the mirror image of q about the flat seabed $z = -H$.

Similarly, when the upper water surface is a free surface of infinite extent, we have the Green function G_F, and the corresponding Fourier transforms $\widehat{G}_F$ and $\tilde{G}_F$ as

$$G_F = G_0 + \frac{1}{\pi}\int_{-\infty}^{+\infty}\int_{-\infty}^{+\infty} e^{i\alpha(\xi-x)}e^{i\beta(\eta-y)}\left[\frac{\hat{C}(k,\zeta)\hat{C}(k,z)}{K_f^{\varepsilon}(\alpha,\beta)} - \frac{\mathcal{N}(\zeta,z)}{k}\right]d\alpha d\beta, \tag{D10}$$

and

$$\widehat{G}_F = \frac{1}{\sqrt{2\pi}}\int_{-\infty}^{+\infty} e^{i\alpha\xi}e^{i\beta(\eta-y)}\frac{e^{-k|\zeta-z|}+e^{-k(\zeta+z+2H)}-2\mathcal{N}(\zeta,z)}{k}d\beta + \frac{2}{\sqrt{2\pi}}\int_{-\infty}^{+\infty} e^{i\alpha\xi}e^{i\beta(\eta-y)}\frac{\hat{C}(k,\zeta)\hat{C}(k,z)}{K_f^{\varepsilon}(\alpha,\beta)}d\beta, \tag{D11}$$

and

$$\tilde{G}_F = 2e^{i\alpha\xi}e^{i\beta\eta}\left[\frac{C(k,\zeta)C(k,z)\tanh(kH) - C(k,z_<)S(k,z_>)}{k} + \frac{\hat{C}(k,\zeta)\hat{C}(k,z)}{K_f^{\varepsilon}(\alpha,\beta)}\right], \tag{D12}$$

or

$$\tilde{G}_F = e^{i\alpha\xi}e^{i\beta\eta}\left[\frac{e^{-k|\zeta-z|}+e^{-k(\zeta+z+2H)}-2\mathcal{N}(\zeta,z)}{k} + 2\frac{\hat{C}(k,\zeta)\hat{C}(k,z)}{K_f^{\varepsilon}(\alpha,\beta)}\right]. \tag{D13}$$

APPENDIX E: FAR-FIELD WAVE COMPONENT OF THE GREEN FUNCTION

We consider the wave component of the Green function, which is written in general form of double Fourier integral as

$$G^W = \lim_{\varepsilon\to 0^+}\int_{-\infty}^{+\infty}\int_{-\infty}^{+\infty}\frac{A(\alpha,\beta)e^{-i(\alpha\bar{x}+\beta\bar{y})}}{K(\alpha,\beta)+i\varepsilon\Psi(\alpha,\beta)}d\alpha d\beta. \tag{E1}$$

This is similar to what was considered by Noblesse and Chen [49]. Here, we follow a different procedure. $K(\alpha,\beta)$ in Eq. (E1) is the dispersion equation for free-surface wave or flexural-gravity wave, and the only importance of the function $\Psi(\alpha,\beta)$ is its sign. We first transform the coordinate system (α,β) to (K,S). Here, $K(\alpha,\beta)$ and $S(\alpha,\beta)$ axes are orthogonal, which gives

$$K_\alpha S_\alpha + K_\beta S_\beta = 0, \tag{E2}$$

where the subscript α (β) indicates the partial derivative with respect to α (β). Then, Eq. (E1) can be rewritten as

$$G^W = \lim_{\varepsilon\to 0^+}\int_{-\infty}^{+\infty}\int_{-\infty}^{+\infty}\frac{Ae^{-i(\alpha\bar{x}+\beta\bar{y})}}{K+i\varepsilon\Psi}J(K,S)dKdS, \tag{E3}$$

where $J(K,S)$ is the Jacobian due to the transformation of the coordinates, and $\alpha = \alpha(K, S)$, $\beta = \beta(K, S)$. The integral with respect to K can be decomposed into two parts, i.e.,

$$I^W = \lim_{\varepsilon\to 0^+} \int_{-\infty}^{+\infty} \frac{Ae^{-i(\alpha\bar{x}+\beta\bar{y})}}{K + i\varepsilon\Psi} J(K,S)dK = I_P^W + I_R^W, \tag{E4}$$

where

$$I_P^W = P.V. \int_{-\infty}^{+\infty} \frac{Ae^{-i(\alpha\bar{x}+\beta\bar{y})}}{K} J(K,S)dK \tag{E5}$$

is due to the principal value (P.V.) of the integral, and

$$I_R^W = -i\pi\,\mathrm{sgn}((\Psi)_{K=0})(A)_{K=0}e^{-\mathrm{i}[\alpha(0,S)\bar{x}+\beta(0,S)\bar{y}]}J(0,S) \tag{E6}$$

is due to the simple pole at $K = 0$. Equation (E5) can be rewritten as

$$I_P^W = \int_{-\infty}^{+\infty} \frac{[A - (A)_{K=0}]e^{-i(\alpha\bar{x}+\beta\bar{y})}}{K} J(K,S)dK + (A)_{K=0} \times P.V. \int_{-\infty}^{+\infty} \frac{e^{-i(\alpha\bar{x}+\beta\bar{y})}}{K} J(K,S)dK. \tag{E7}$$

The integrand of the first integral is nonsingular. As $r = \sqrt{\xi^2 + \beta^2} \to \infty$, the stationary-phase method can show that it decays at a rate of $1/\sqrt{r}$. For the second one, the contribution to the result will mainly be from the singular point, $K = 0$. We may introduce

$$\varphi = (\alpha\bar{x} + \beta\bar{y})/r, \tag{E8}$$

and expand this near $K = 0$ or

$$\varphi = (\varphi)_{K=0} + (\varphi_K)_{K=0}K + (\varphi_{KK})_{K=0}K^2/2 + \cdots, \tag{E9}$$

where $\varphi_K = \partial\varphi/\partial K$, and $\varphi_{KK} = \partial^2\varphi/\partial K^2$. Substituting Eq. (E8) into the second integral of (E7), and ignoring the higher-order terms, we have

$$\begin{aligned}\lim_{r\to\infty} P.V. \int_{-\infty}^{+\infty} \frac{e^{-i(\alpha\bar{x}+\beta\bar{y})}}{K} J(K,S)dK &\approx \lim_{r\to\infty} e^{-i(\varphi)_{K=0}r} P.V. \int_{-\infty}^{+\infty} \frac{e^{-i(\varphi_K)_{K=0}rK}}{K} J(K,S)dK \\ &\approx -i\pi[\mathrm{sgn}(\varphi_K)J(K, S)e^{-ir\varphi}]_{K=0}.\end{aligned} \tag{E10}$$

Invoking Eq. (E10), we obtain that

$$\lim_{r\to\infty} I_P^W \approx -i\pi\,\mathrm{sgn}[(\varphi_K)_{K=0}]AJ(0, S)e^{-ir(\varphi)_{K=0}}. \tag{E11}$$

Because S now represents the dispersion curves of $K(\alpha, \beta) = 0$ in the Fourier plane, by using

$$\varphi_K = \frac{(\nabla\varphi)(\nabla K)}{|\nabla K|^2} \tag{E12}$$

we have

$$\varphi_K = \frac{\bar{x}K_\alpha + \bar{y}K_\beta}{r|\nabla K|^2}(K = 0), \tag{E13}$$

which provides

$$\mathrm{sgn}(\varphi_K) = \mathrm{sgn}(\bar{x}K_\alpha + \bar{y}K_\beta)\,(K = 0). \tag{E14}$$

Substituting Eqs. (E6) and (E11) into Eq. (E3), and using Eq. (E14), we have

$$\lim_{r\to\infty} G^W \approx -i\pi \sum_{m=1}^{M} \int_{S_m} [\mathrm{sgn}(\bar{x}K_\alpha + \bar{y}K_\beta) + \mathrm{sgn}(\Psi)]AJ(0, S)e^{-i(\alpha\bar{x}+\beta\bar{y})}dS, \tag{E15}$$

where S_m represents the mth segment of the dispersion curve in the (α, β) plane. Substituting the following equation [49]

$$J = \frac{1}{|\nabla K|}, \quad (K = 0) \tag{E16}$$

into (E15), we have

$$\lim_{r\to\infty} G^W \approx -i\pi \sum_{m=1}^{M} \int_{S_m} [\mathrm{sgn}(\bar{x}K_\alpha + \bar{y}K_\beta) + \mathrm{sgn}(\Psi)] \frac{Ae^{-i(\alpha\bar{x}+\beta\bar{y})}}{|\nabla K|} dS. \tag{E17}$$

It may be noticed that Eq. (E17) is identical to Eq. (27b) of Noblesse and Chen [49].

[1] M. Casas-Prat and X. L. Wang, Projections of extreme ocean waves in the Arctic and potential implications for coastal inundation and erosion, J. Geophys. Res.: Oceans **125**, e2019JC015745 (2020).

[2] Y. Aksenov, E. E. Popova, A. Yool, A. J. G. Nurser, T. D. Williams, L. Bertino, and J. Bergh, On the future navigability of Arctic sea routes: High-resolution projections of the Arctic Ocean and sea ice, Mar. Policy **75**, 300 (2017).

[3] G. Q. Robin, Wave propagation through fields of pack ice, Philos. Trans. R. Soc. **A255**, 313 (1963).

[4] V. A. Squire, Ocean wave interactions with sea ice: A reappraisal, Annu. Rev. Fluid Mech. **52**, 37 (2020).

[5] J. V. Wehausen and E. V. Laitone, *Surface Waves*, Handbuch des Physik (Springer Verlag, Berlin, 1960).

[6] P. A. Milewski, J. M. Vanden-Broeck, and Z. Wang, Hydroelastic solitary waves in deep water, J. Fluid Mech. **679**, 628 (2011).

[7] C. Fox and V. A. Squire, Reflection and transmission characteristics at the edge of shore fast sea ice, J. Geophys. Res.: Oceans **95**, 11629 (1990).

[8] C. Fox and V. A. Squire, Strain in shore fast ice due to incoming ocean waves and swell, J. Geophys. Res.: Oceans **96**, 4531 (1991).

[9] C. Fox and V. A. Squire, On the oblique reflexion and transmission of ocean waves at shore fast sea ice, Philos. Trans. R. Soc. A**347**, 185 (1994).

[10] T. Sahoo, T. L. Yip, and A. T. Chwang, Scattering of surface waves by a semi-infinite floating elastic plate, Phys. Fluids **13**, 3215 (2001).

[11] A. Chakrabarti, On the solution of the problem of scattering of surface–water waves by the edge of an ice cover, Proc. R. Soc. London A **456**, 1087 (2000).

[12] N. J. Balmforth and R. V. Craster, Ocean waves and ice sheets, J. Fluid Mech. **395**, 89 (1999).

[13] L. A. Tkacheva, The diffraction of surface waves by a floating elastic plate at oblique incidence, J. Appl. Math. Mech. **68**, 425 (2004).

[14] C. M. Linton and H. Chung, Reflection and transmission at the ocean/sea-ice boundary, Wave Motion **38**, 43 (2003).

[15] K. Eliasson, G. F. Ulfarsson, T. Valsson, and S. M. Gardarsson, Identification of development areas in a warming Arctic with respect to natural resources, transportation, protected areas, and geography, Futures **85**, 14 (2017).

[16] I. V. Sturova, Radiation of waves by a cylinder submerged in water with ice floe or polynya, J. Fluid Mech. **784**, 373 (2015).

[17] I. V. Sturova and L. A. Tkacheva, Wave radiation by a cylinder submerged in water with an ice floe or a polynya, in *The 30th International Workshop on Water Waves and Floating Bodies* (IWWWFB, Bristol, UK, 2015).

[18] K. Ren, G. X. Wu, and G. A. Thomas, Wave excited motion of a body floating on water confined between two semi-infinite ice sheets, Phys. Fluids **28**, 127101 (2016).

[19] Z. F. Li, Y. Y. Shi, and G. X. Wu, Interaction of waves with a body floating on polynya between two semi-infinite ice sheets, J. Fluids Struct. **78**, 86 (2018).

[20] Z. F. Li, Y. Y. Shi, and G. X. Wu, Interaction of wave with a body floating on a wide polynya, Phys. Fluids **29**, 097104 (2017).
[21] K. Ren, G. X. Wu, and C. Y. Ji, Wave diffraction and radiation by a vertical circular cylinder standing in a three-dimensional polynya, J. Fluids Struct. **82**, 287 (2018).
[22] Z. F. Li, Y. Y. Shi, and G. X. Wu, A hybrid method for linearized wave radiation and diffraction problem by a three dimensional floating structure in a polynya, J. Comput. Phys. **412**, 109445 (2020).
[23] Z. F. Li, G. X. Wu, and K. Ren, Interactions of waves with a body floating in an open water channel confined by two semi-infinite ice sheets, J. Fluid Mech. **917**, A19 (2021).
[24] Z. F. Li and G. X. Wu, Hydrodynamic force on a ship floating on the water surface near a semi-infinite ice sheet, Phys. Fluids **33**, 127101 (2021).
[25] H. Liang and X. B. Chen, Asymptotic analysis of capillary–gravity waves generated by a moving disturbance, Eur. J. Mech. B Fluids **72**, 624 (2018).
[26] M. Rabaud and F. Moisy, Ship wakes: Kelvin or Mach angle? Phys. Rev. Lett. **110**, 214503 (2013).
[27] A. Darmon, M. Benzaquen, and E. Raphaël, Kelvin wake pattern at large Froude numbers, J. Fluid Mech. **738**, R3 (2014).
[28] J. W. Davys, R. J. Hosking, and A. D. Sneyd, Waves due to a steadily moving source on a floating ice plate, J. Fluid Mech. **158**, 269 (1985).
[29] T. Takizawa, Deflection of a floating sea ice sheet induced by a moving load, Cold Reg. Sci. Technol. **11**, 171 (1985).
[30] F. Milinazzo, M. Shinbrot, and N. W. Evans, A mathematical analysis of the steady response of floating ice to the uniform motion of a rectangular load, J. Fluid Mech. **287**, 173 (1995).
[31] K. A. Shishmarev, T. I. Khabakhpasheva, and A. A. Korobkin, The ice response to an oscillating load moving along a frozen channel, IOP Conf. Ser.: Earth Environ. Sci. **193**, 012072 (2018).
[32] L. A. Tkacheva, Behavior of a semi-infinite ice cover under a uniformly moving load, J. Appl. Mech. Tech. Phys. **59**, 258 (2018).
[33] L. A. Tkacheva, Wave motion in an ice sheet with crack under uniformly moving load, Fluid Dyn. **54**, 14 (2019).
[34] I. V. Sturova and L. A. Tkacheva, Movement of external load over free surface of fluid in the ice channel, J. Phys. Conf. Ser. **1268**, 012066 (2019).
[35] S. P. Timoshenko and K. S. Woinowsky, *Theory of Plates and Shells* (McGraw-Hill, Singapore, 1959).
[36] J. Lighthill, *Waves in Fluids* (Cambridge University Press, Cambridge, 1978).
[37] B. Noble, *Methods Based on the Wiener-Hopf Technique for the Solution of Partial Differential Equations* (Pergamon Press, London, 1958).
[38] X. B. Chen and G. X. Wu, On singular and highly oscillatory properties of the Green function for ship motions, J. Fluid Mech. **445**, 77 (2001).
[39] H. Liang and X. B. Chen, Viscous effects on the fundamental solution to ship waves, J. Fluid Mech. **879**, 744 (2019).
[40] V. A. Squire, J. P. Dugan, P. Wadhams, P. J. Rottier, and A. K. Liu, Of ocean waves and sea ice, Annu Rev Fluid Mech **27**, 115 (1995).
[41] O. M. Faltinsen, *Hydrodynamics of High-Speed Marine Vehicles* (Cambridge University Press, New York, 2005).
[42] J. Thomson, Y. L. Fan, S. Stammerjohn, J. Stopa, W. E. Rogers, F. Girard-Ardhuin, F. Ardhuin, H. L. Shen, W. Perrie, H. Shen *et al.*, Emerging trends in the sea state of the Beaufort and Chukchi seas, Ocean Modell. **105**, 1 (2016).
[43] D. V. Evans and R. Porter, Wave scattering by narrow cracks in ice sheets floating on water of finite depth, J. Fluid Mech. **484**, 143 (2003).
[44] P. Brocklehurst, A. A. Korobkin, and E. I. Părău, Interaction of hydro-elastic waves with a vertical wall, J. Eng. Math. **68**, 215 (2010).
[45] A. A. Korobkin, S. Malenica, and T. Khabakhpasheva, Interaction of flexural-gravity waves in ice cover with vertical walls, Philos. Trans. R. Soc. A**376**, 20170347 (2018).

[46] X. B. Chen, Peculiar properties of ship-motion Green functions in water of finite depth, in *The 15th International Workshop on Water Waves and Floating Bodies* (IWWWFB, Caesarea, Israel, 2000).

[47] G. X. Wu, Radiation and diffraction by a submerged sphere advancing in water waves of finite depth, Proc. R. Soc. London A **448**, 29 (1995).

[48] X. B. Chen and F. Noblesse, Dispersion relation and far-field waves, in *The 12th International Workshop on Water Waves and Floating Bodies* (IWWWFB, Marseille, France, 1997).

[49] F. Noblesse and X. B. Chen, Decomposition of free-surface effects into wave and near-field components, Ship Technol. Res. **42**, 167 (1995).